Supplementary Information

Aryl bismuth phosphinates [$BiAr_2(O(O)PRR')$]: structure-activity relationships for antibacterial activity and cytotoxicity

Megan E. Herdman, Melissa V. Werrett and Philip C. Andrews

School of Chemistry, Monash University, Clayton, Melbourne, VIC 3800, Australia.

Contents

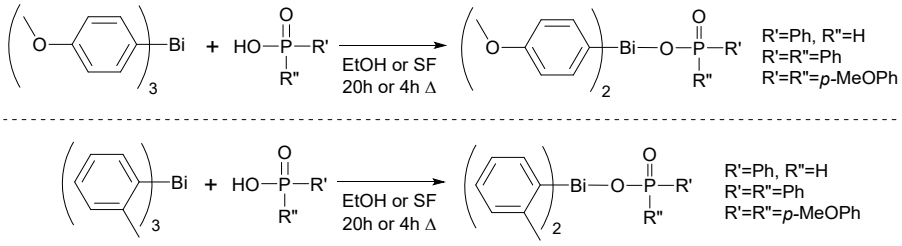

Scheme S1 Attempted solvent mediated and solvent free routes to form diaryl bismuth *mono*-phosphinato complexes.

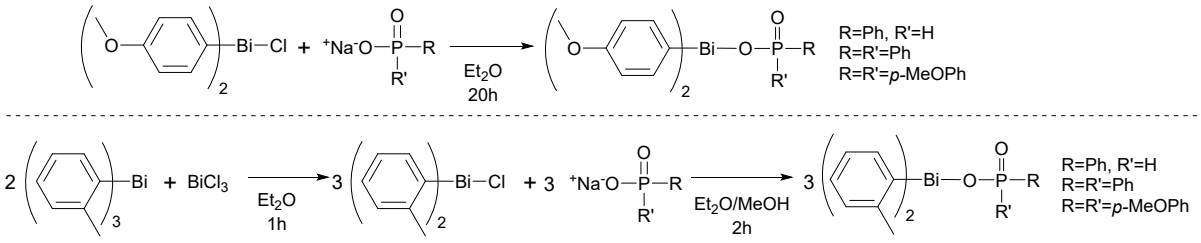

Scheme S2 Attempted salt metathesis route to form diaryl bismuth *mono*-phosphinato complexes.

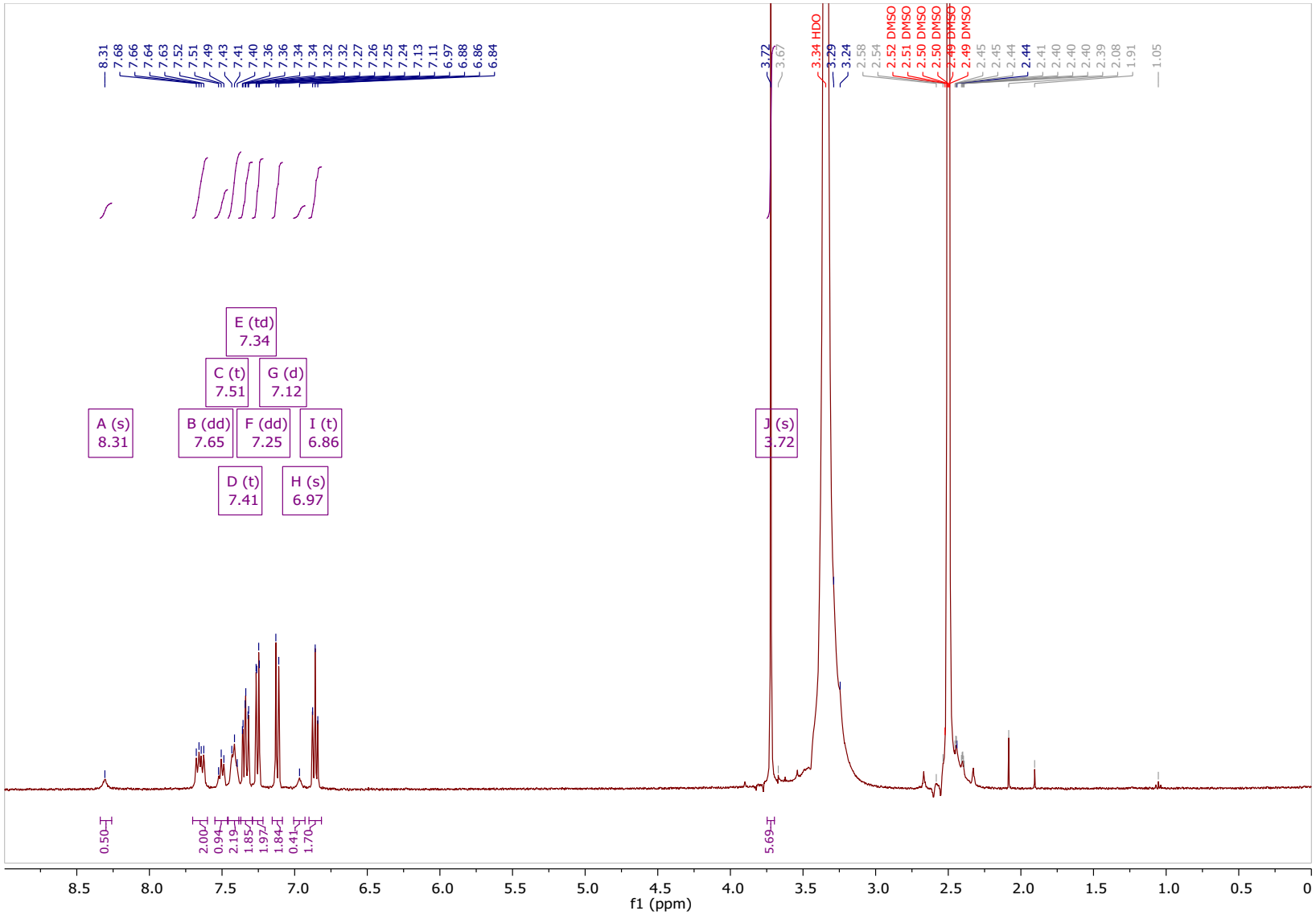

Figure S1 ^{1}H NMR spectrum of complex [Bi(*o*-MeOPh)$_2$(O(O)P(H)Ph)]$_n$ **1** in d$_6$-DMSO.

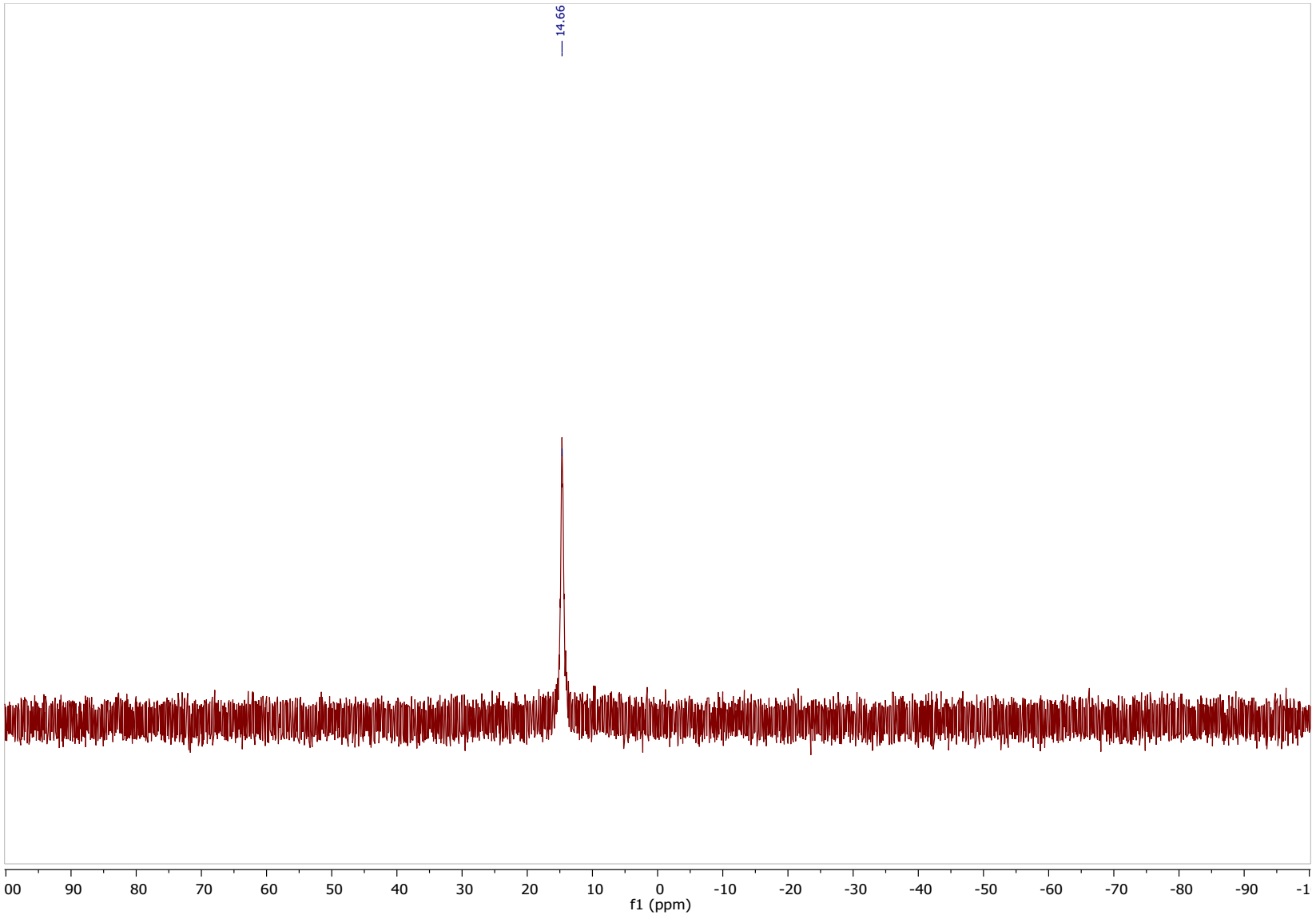

Figure S2 ^{31}**P** NMR spectrum of complex [Bi(*o*-MeOPh)$_2$(O(O)P(H)Ph)]$_n$ **1** in d$_6$-DMSO.

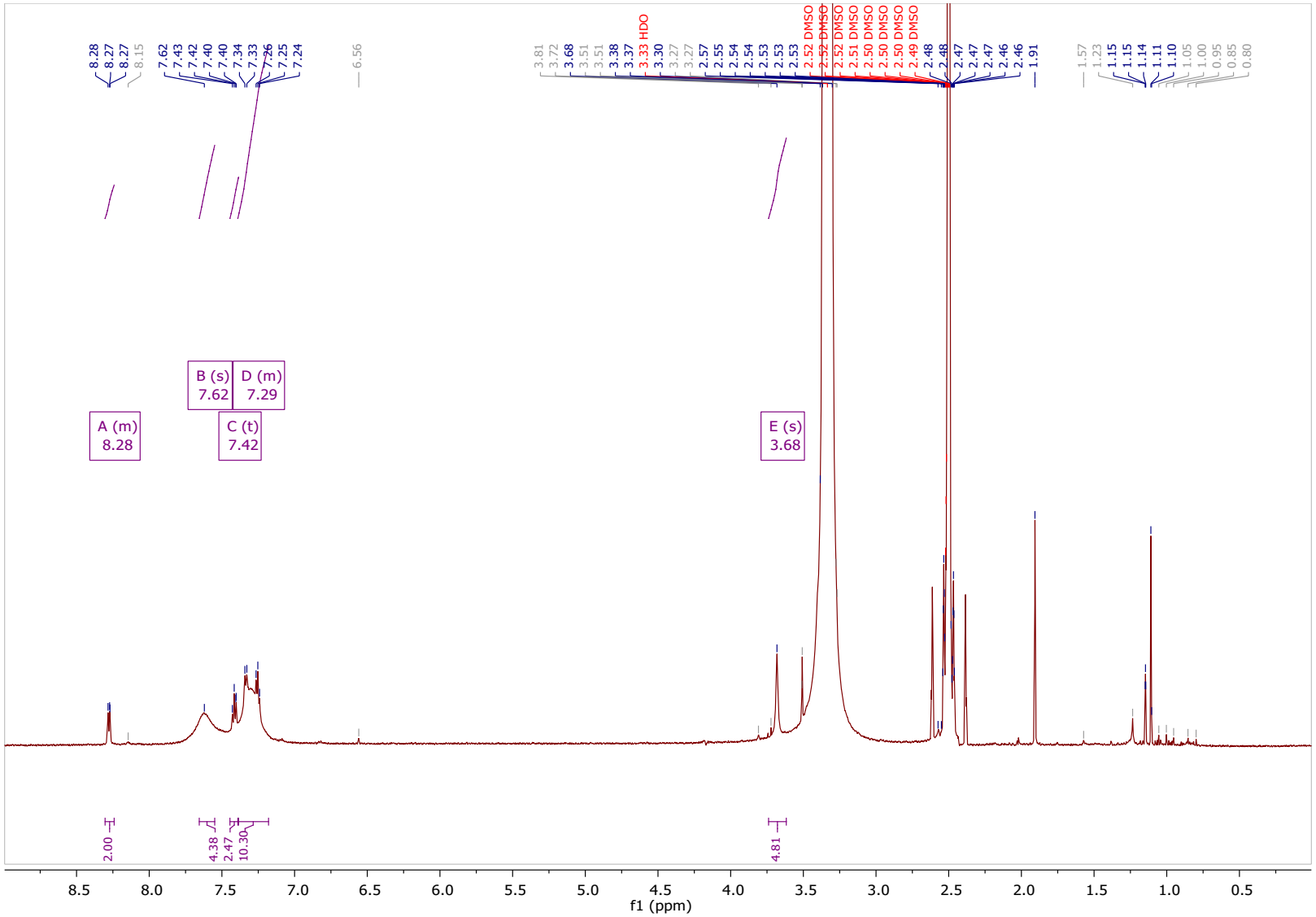

Figure S3 ^{1}H NMR spectrum of complex [Bi(*o*-MeOPh)$_2$(O(O)PPh$_2$)]$_n$ **2** in d$_6$-DMSO.

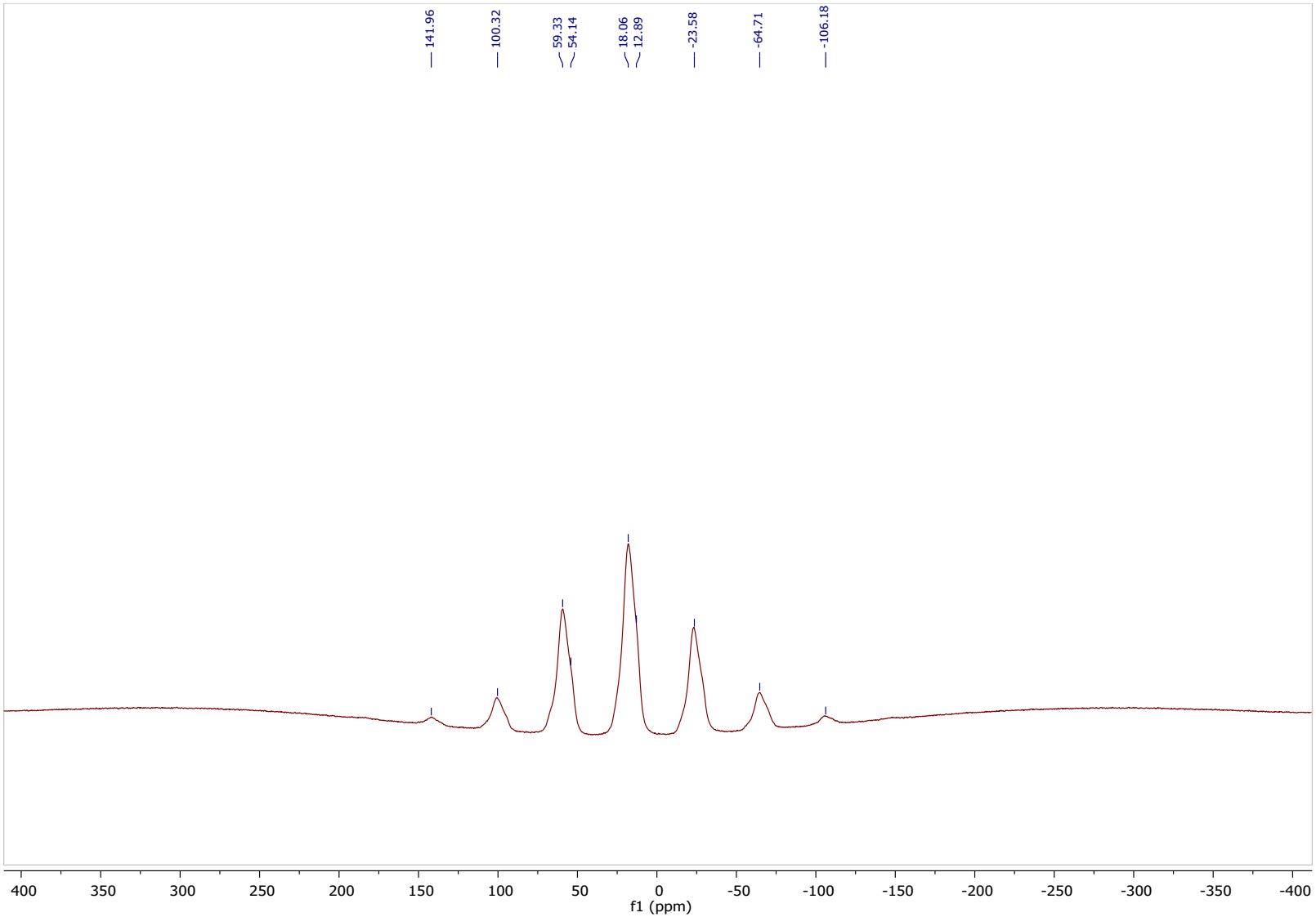

Figure S4 Solid state ^{31}P NMR spectrum of complex [Bi(*o*-MeOPh)$_2$(O(O)PPh$_2$)]$_n$ **2**.

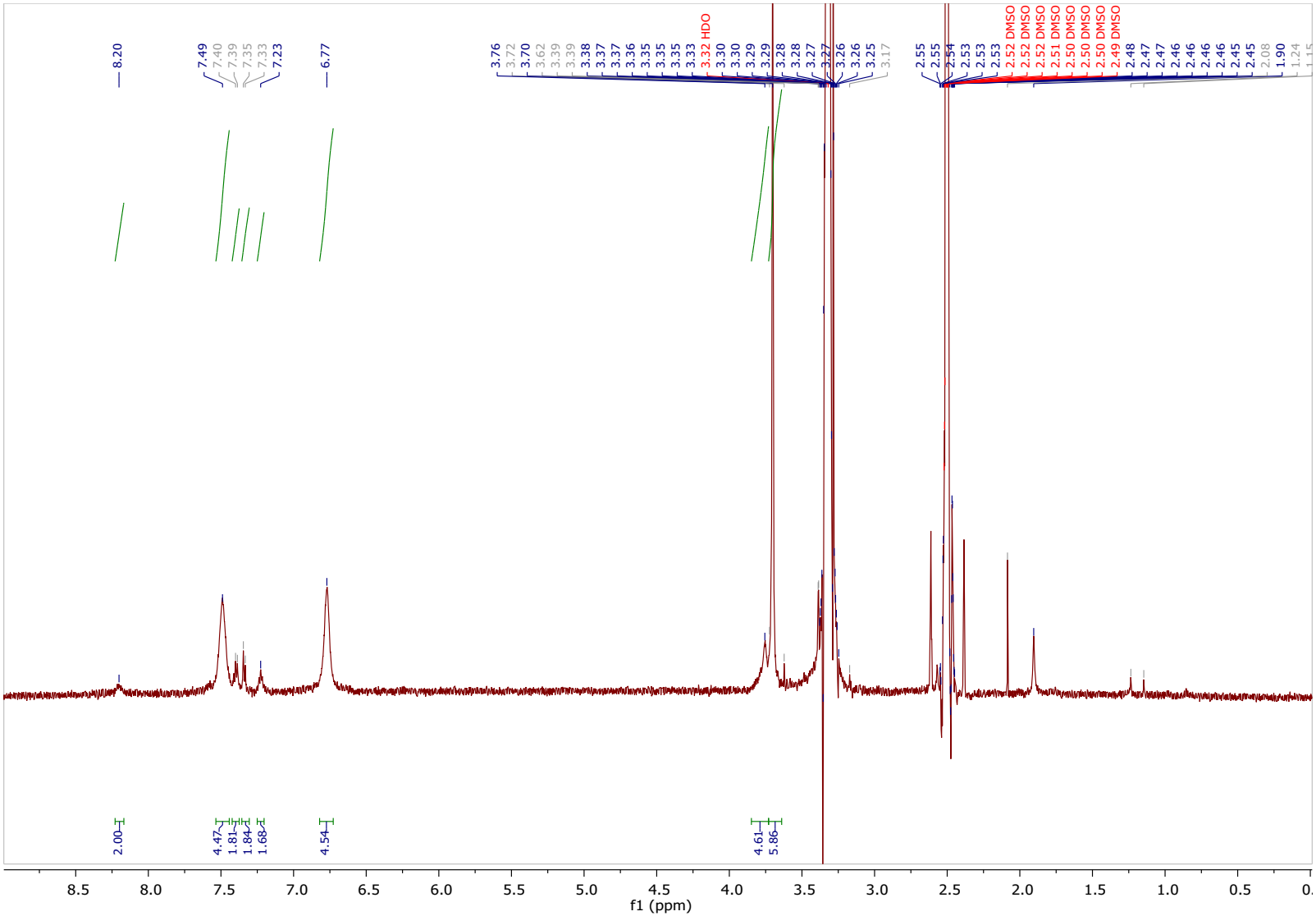

Figure S5 ^{1}H NMR spectrum of complex [Bi(*o*-MeOPh)$_2$(O(O)P(*p*-MeOPh)$_2$)]$_n$ **3** in d$_6$-DMSO.

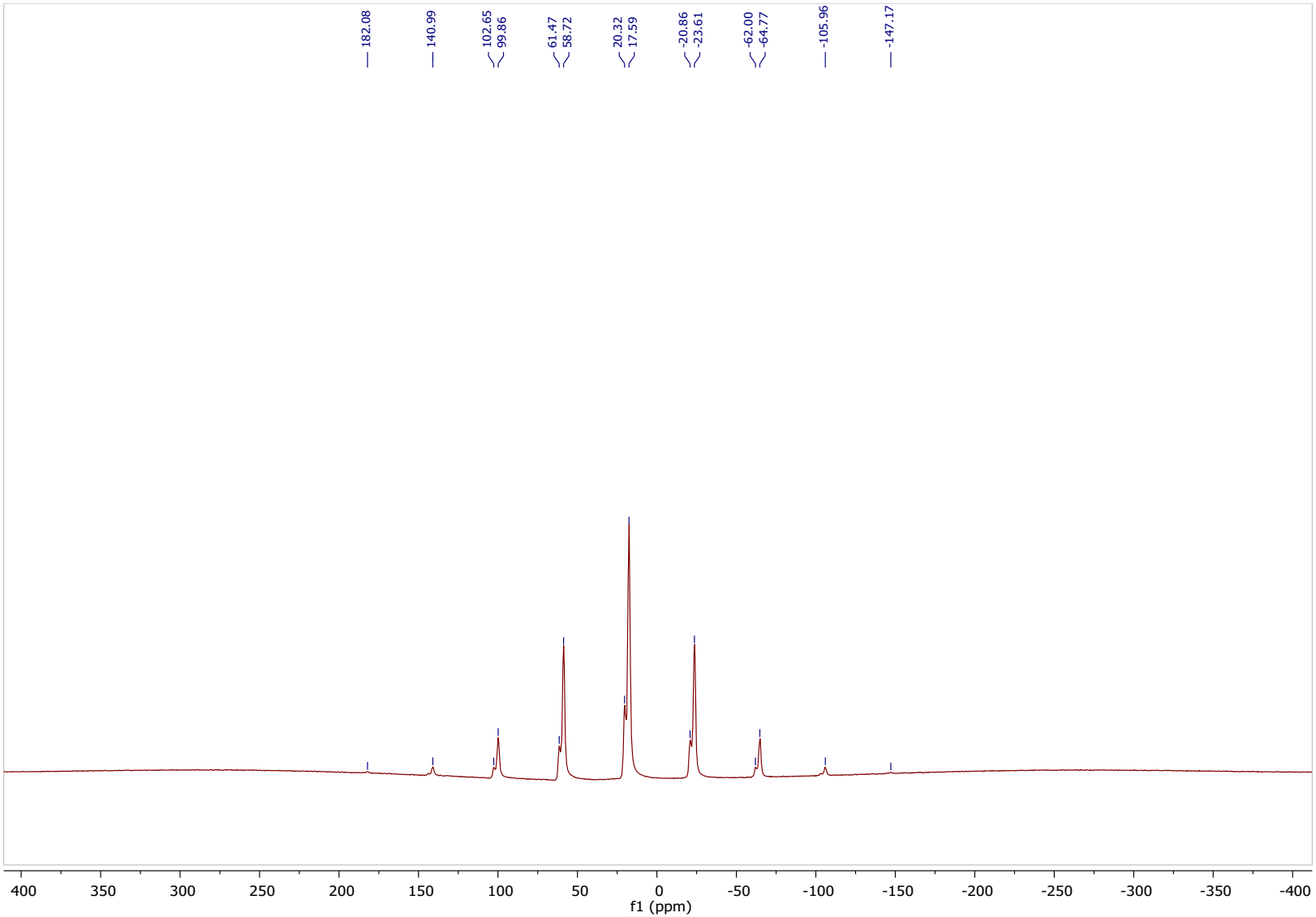

Figure S6 Solid state ^{31}P NMR spectrum of complex [Bi(*o*-MeOPh)$_2$(O(O)P(*p*-MeOPh)$_2$)]$_n$ **3**.

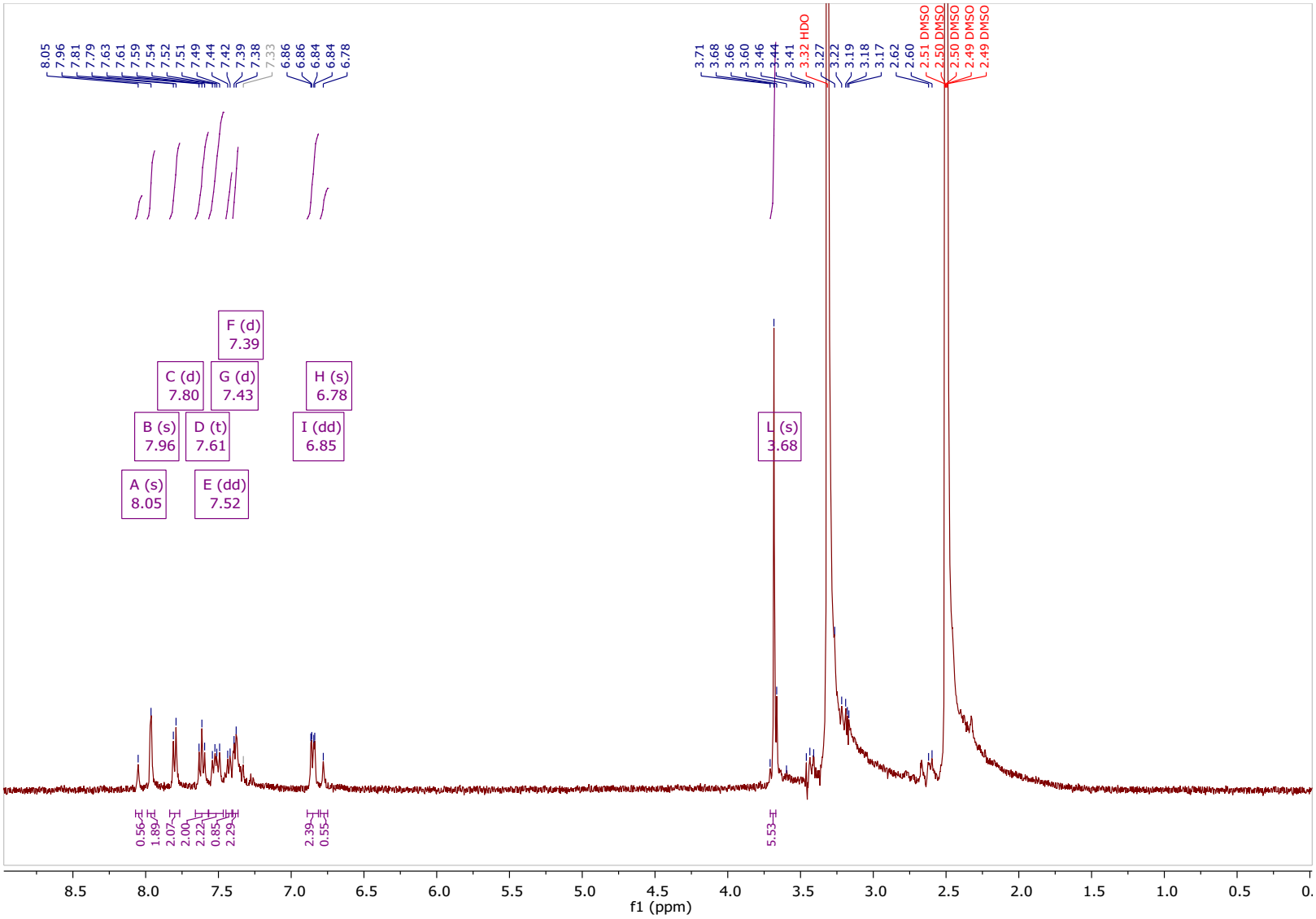

Figure S7 ^{1}H NMR spectrum of complex [Bi(*m*-MeOPh)$_2$(O(O)P(H)Ph)]$_n$ **4** in d$_6$-DMSO.

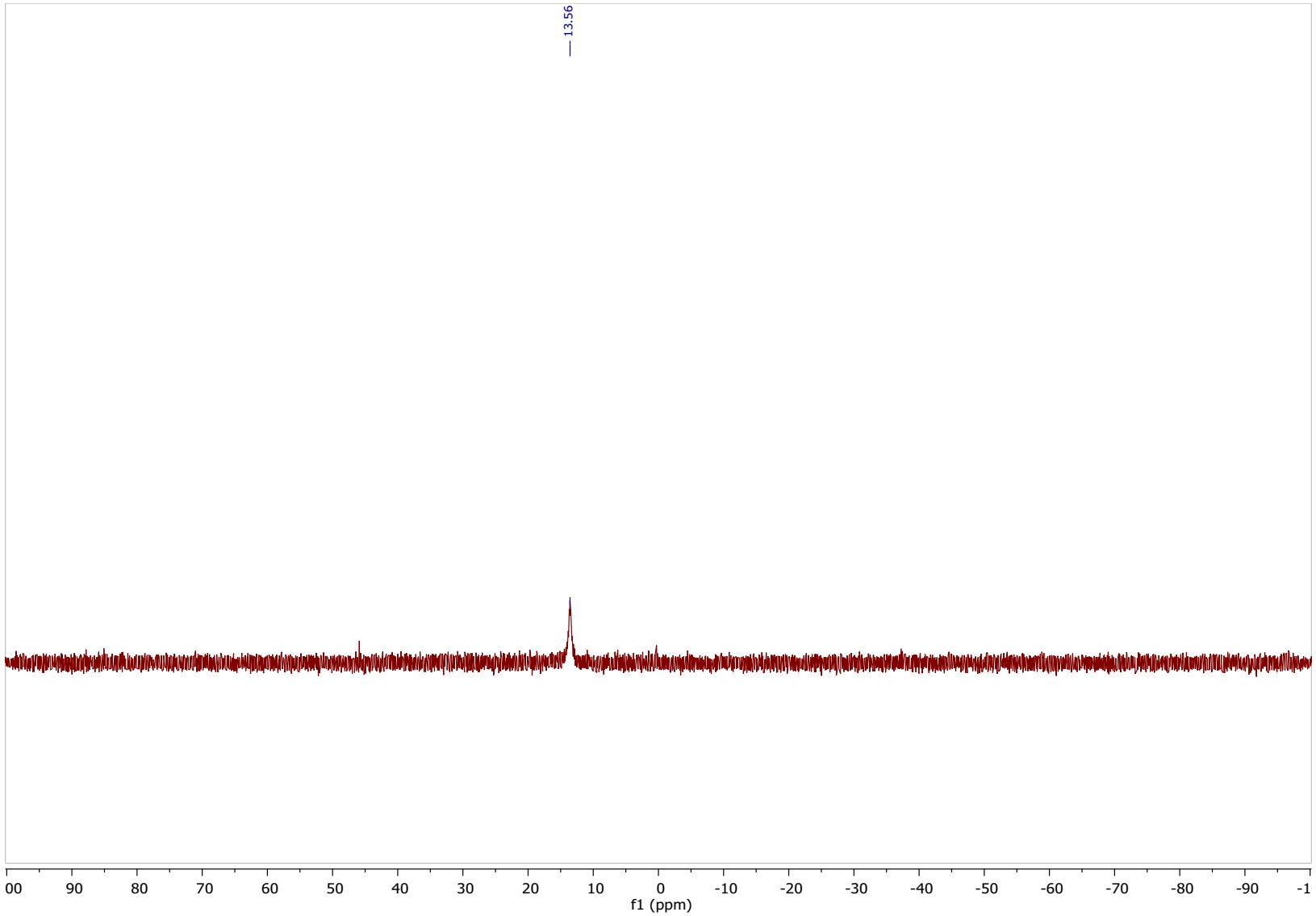

Figure S8 ^{31}P NMR spectrum of complex [Bi(*m*-MeOPh)$_2$(O(O)P(H)Ph)]$_n$ **4** in d$_6$-DMSO.

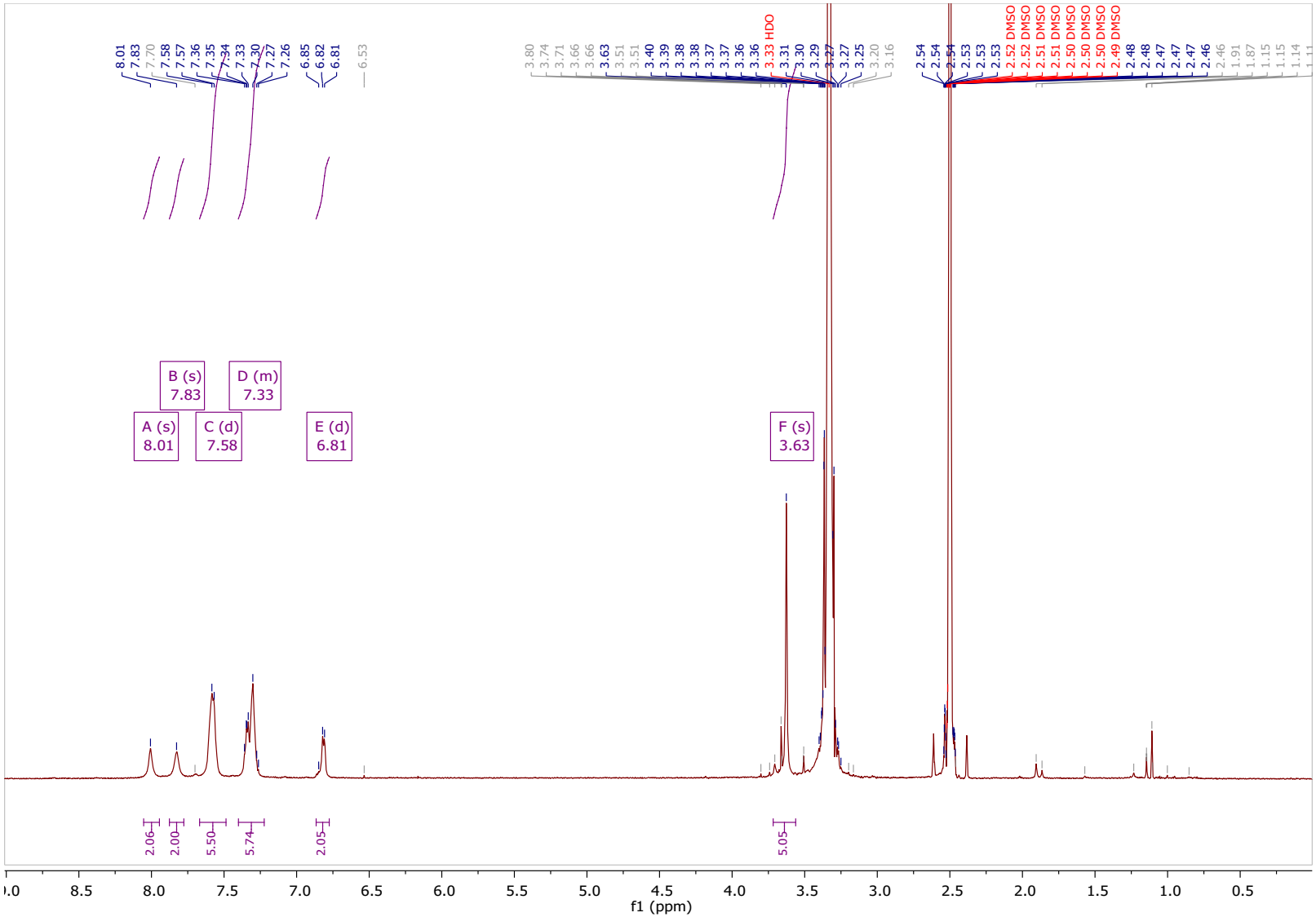

Figure S9 ^{1}H NMR spectrum of complex $[Bi(m\text{-}MeOPh)_2(O(O)PPh_2)]_n$ **5** in d_6-DMSO.

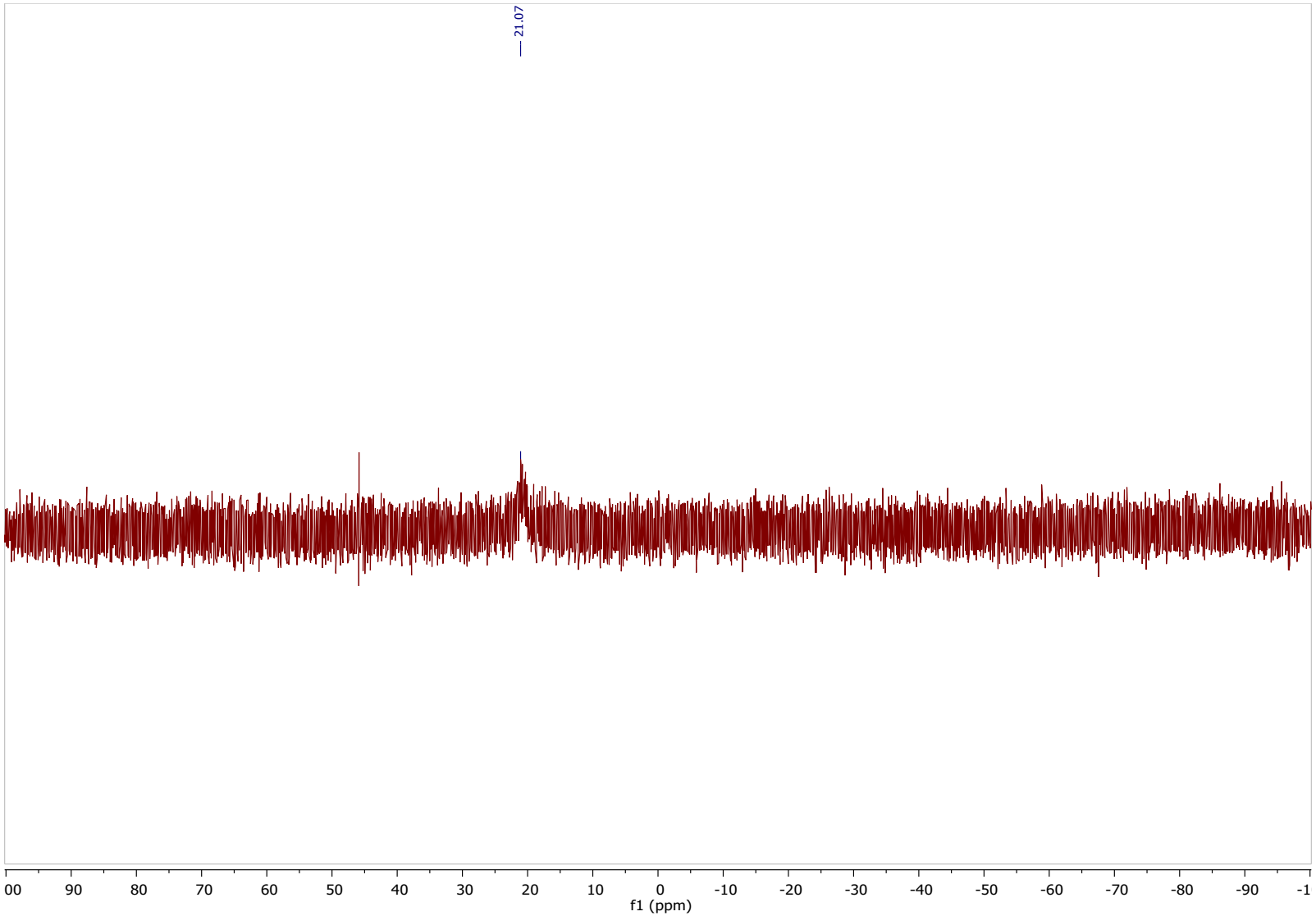

Figure S10 ^{31}P NMR spectrum of complex [Bi(*m*-MeOPh)$_2$(O(O)PPh$_2$)]$_n$ **5** in d$_6$-DMSO.

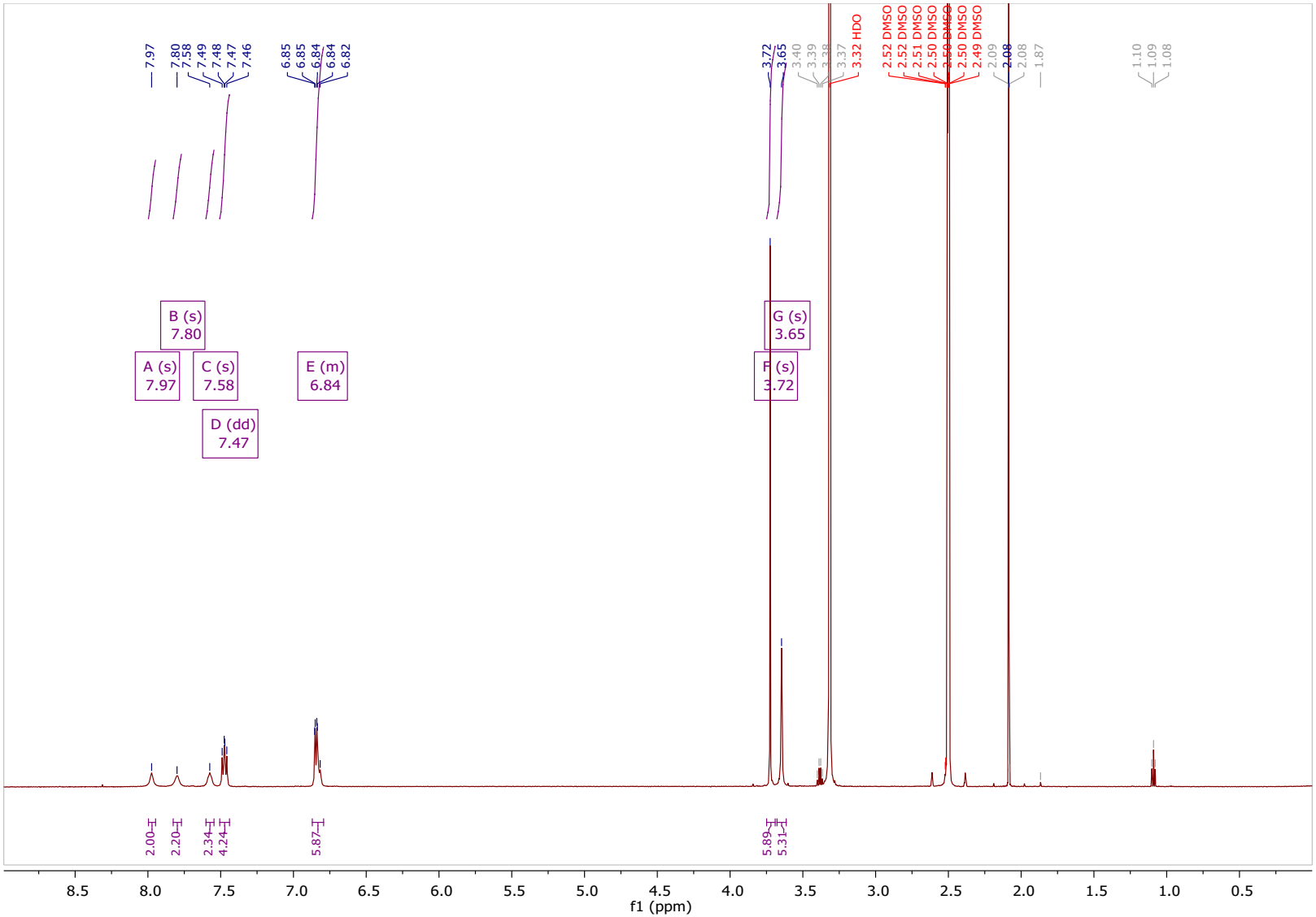

Figure S11 ^{1}H NMR spectrum of complex [Bi(*m*-MeOPh)$_2$(O(O)P(*p*-MeOPh)$_2$)]$_n$ **6** in d$_6$-DMSO. Traces of acetone and Et$_2$O can be observed after washing.

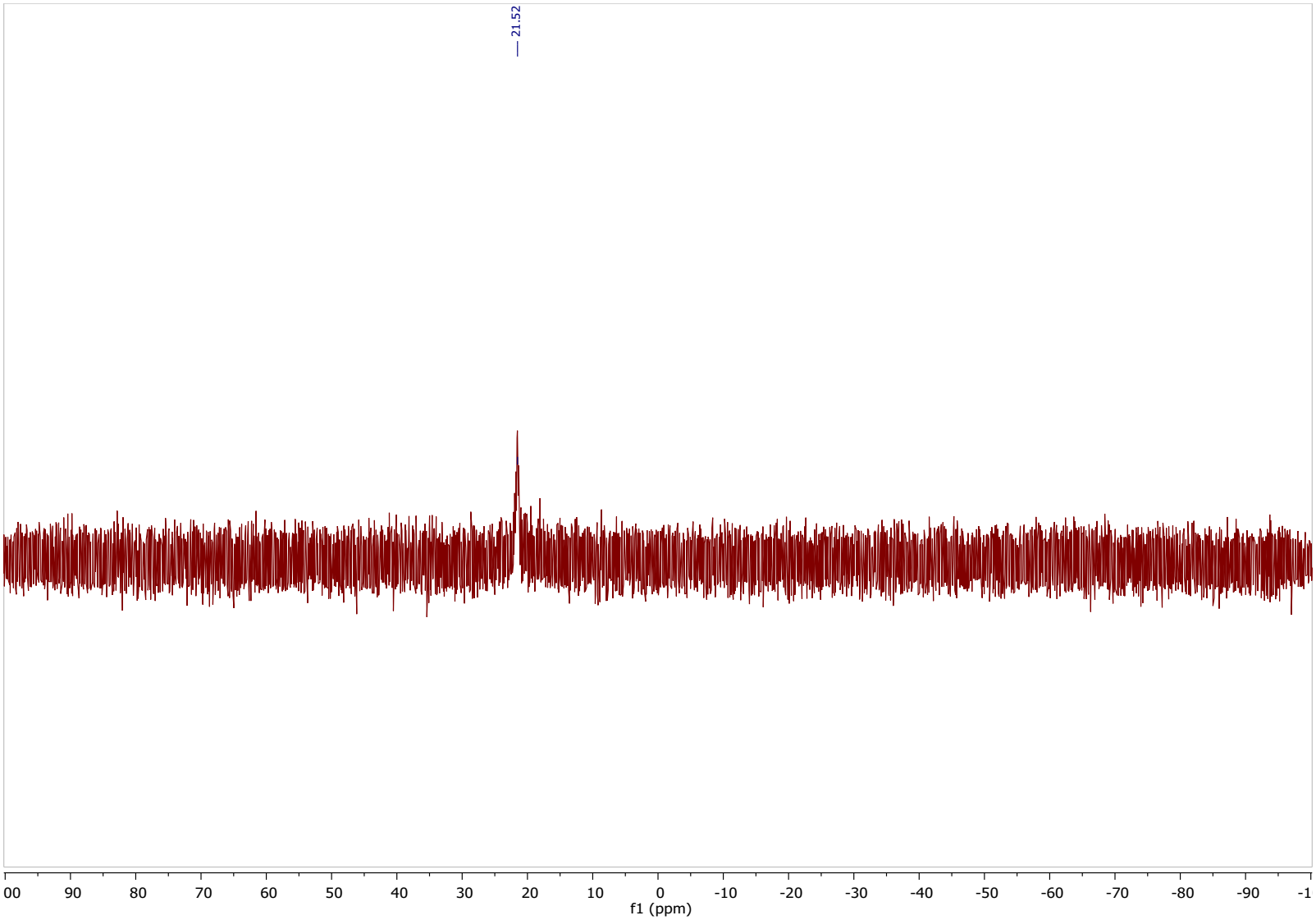

Figure S12 ^{31}P NMR spectrum of complex [Bi(*m*-MeOPh)$_2$(O(O)P(*p*-MeOPh)$_2$)]$_n$ **6** in d$_6$-DMSO.

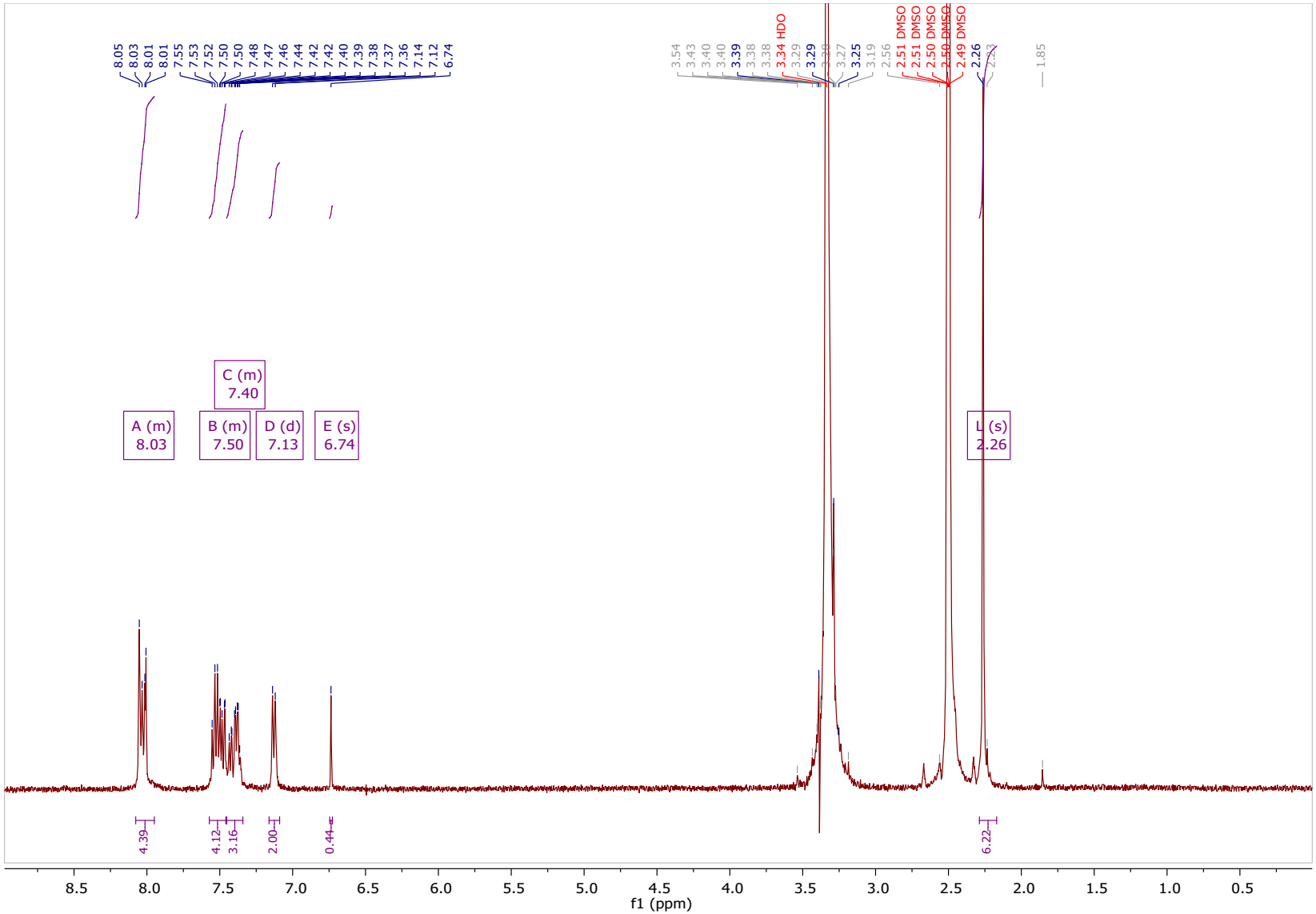

Figure S13 ^{1}H NMR spectrum of complex [Bi(*m*-tol)$_2$(O(O)P(H)Ph)]$_n$ **7** in d$_6$-DMSO.

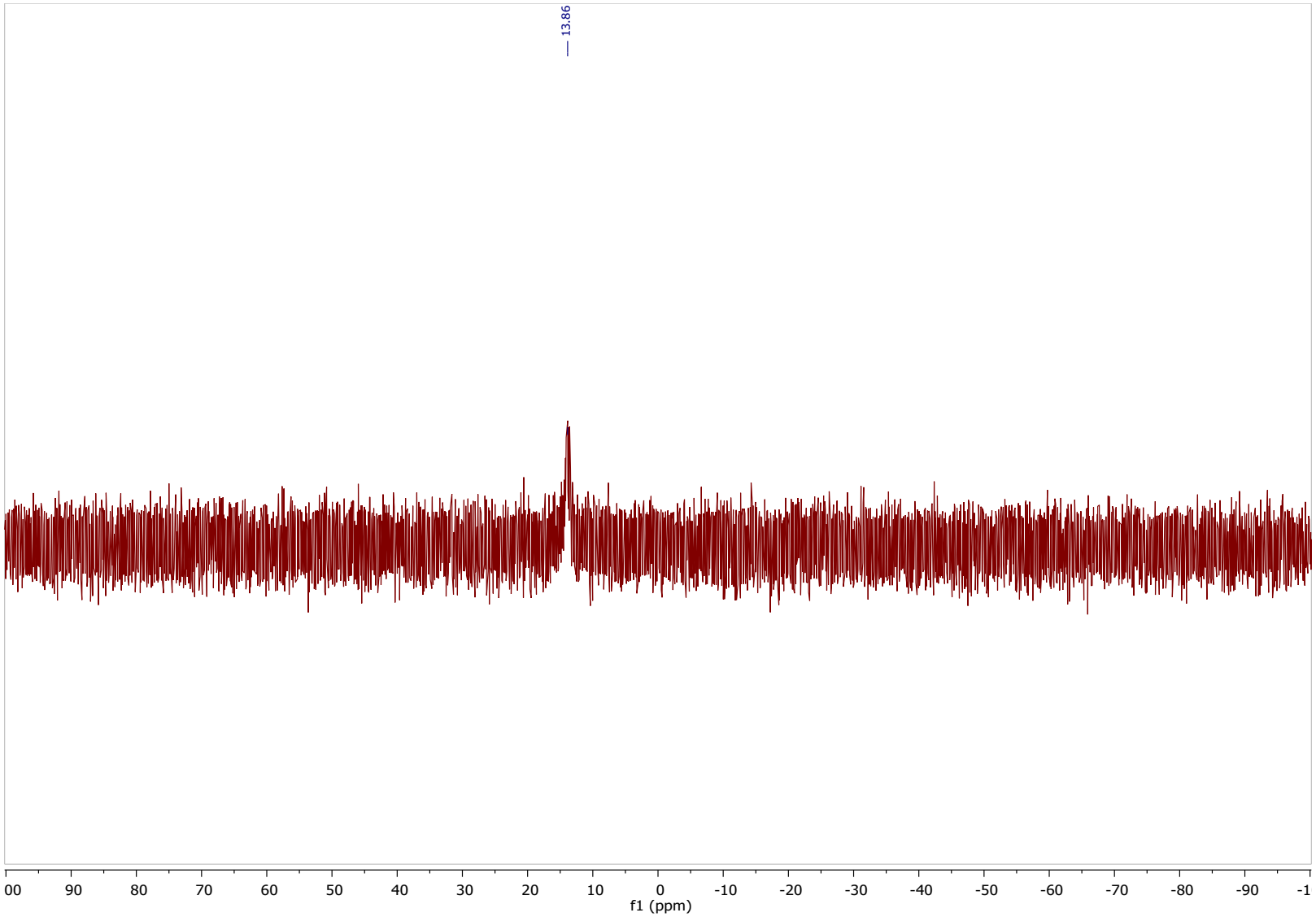

Figure S14 ^{31}P NMR spectrum of complex [Bi(*m*-tol)$_2$(O(O)P(H)Ph)]$_n$ **7** in d$_6$-DMSO.

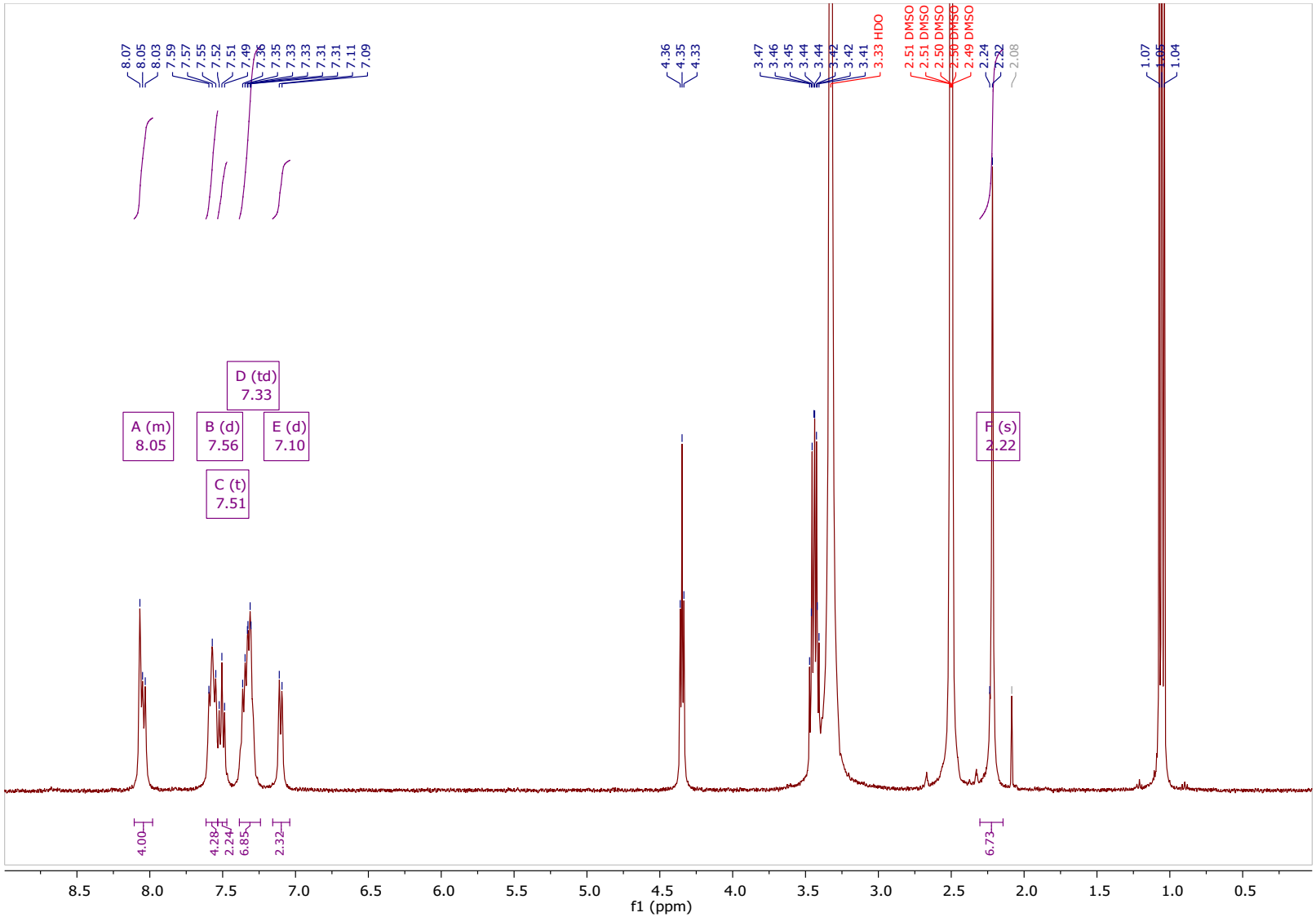

Figure S15 ^{1}H NMR spectrum of complex ([Bi(*m*-tol)$_2$(O(O)PPh$_2$)].DMSO)$_n$ **8** in d$_6$-DMSO. Traces of acetone and ethanol can be observed after washing.

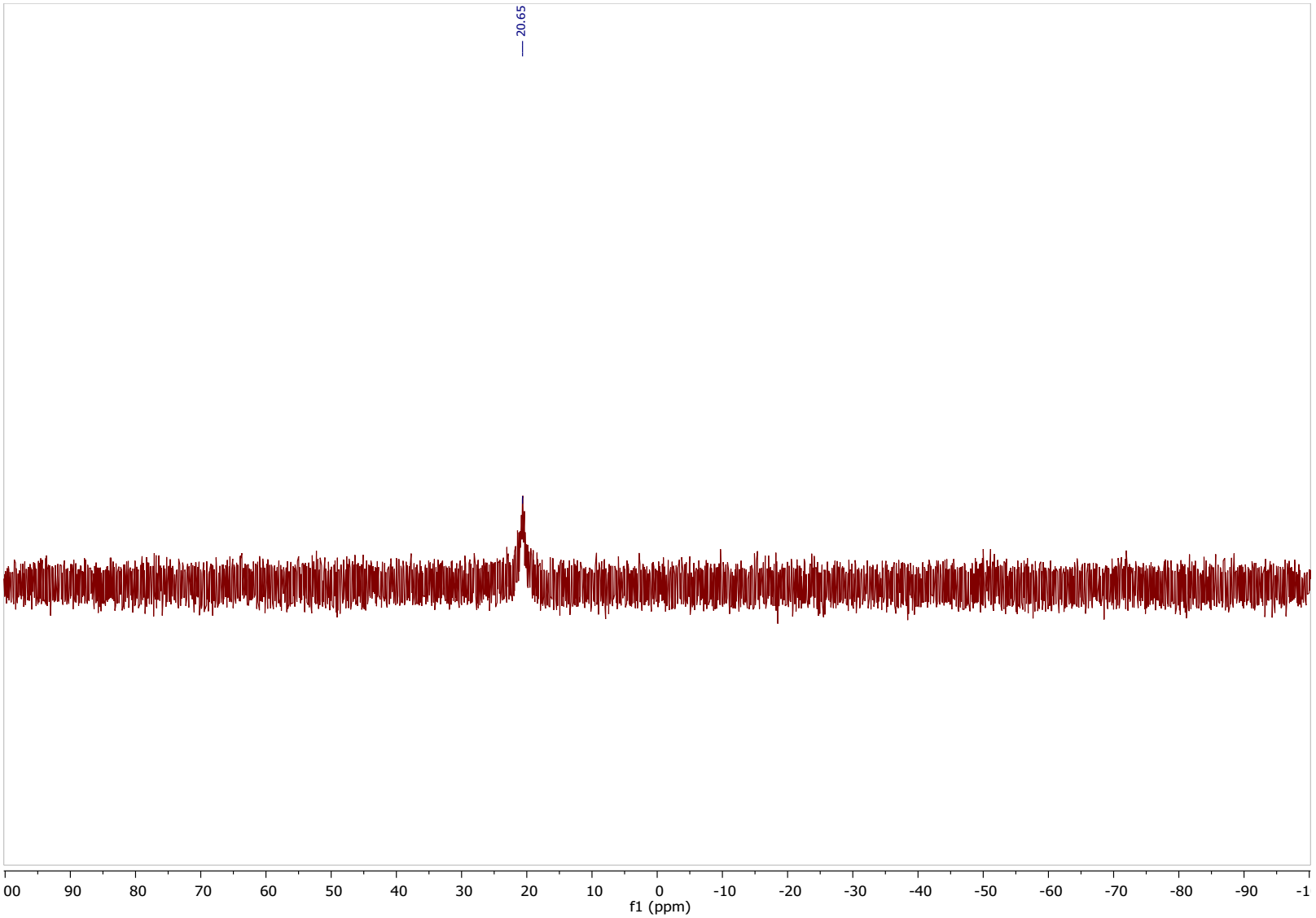

Figure S16 ^{31}P NMR spectrum of complex [Bi(*m*-tol)$_2$(O(O)PPh$_2$)]$_n$ **8** in d$_6$-DMSO.

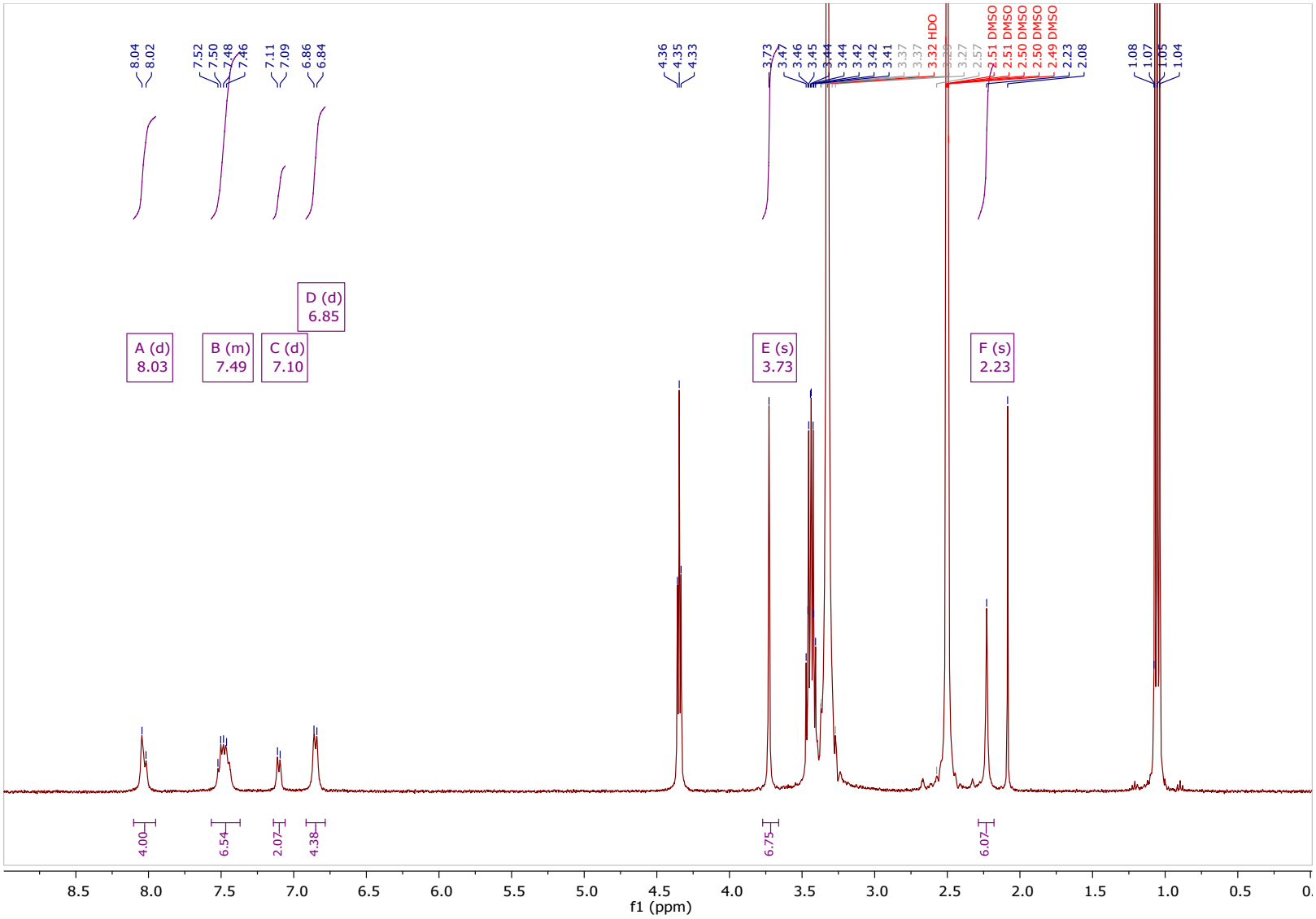

Figure S17 ^{3}H NMR spectrum of complex [Bi(*m*-tol)$_2$(O(O)P(*p*-MeOPh)$_2$)]$_n$ **9** in d$_6$-DMSO. Traces of acetone and ethanol can be observed after washing.

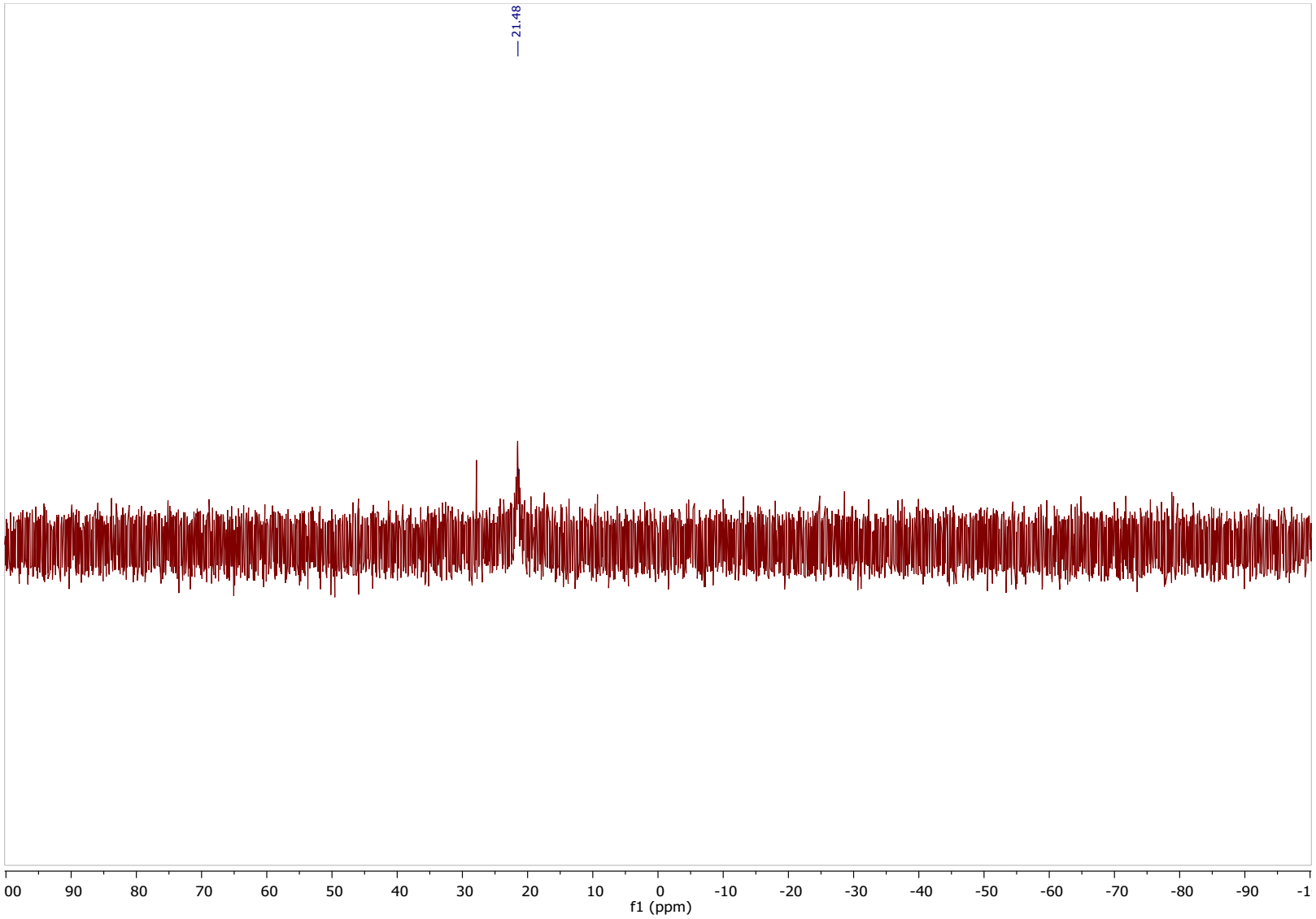

Figure S18 ^{31}P NMR spectrum of complex [Bi(*m*-tol)$_2$(O(O)P(*p*-MeOPh)$_2$)]$_n$ **9** in d$_6$-DMSO.

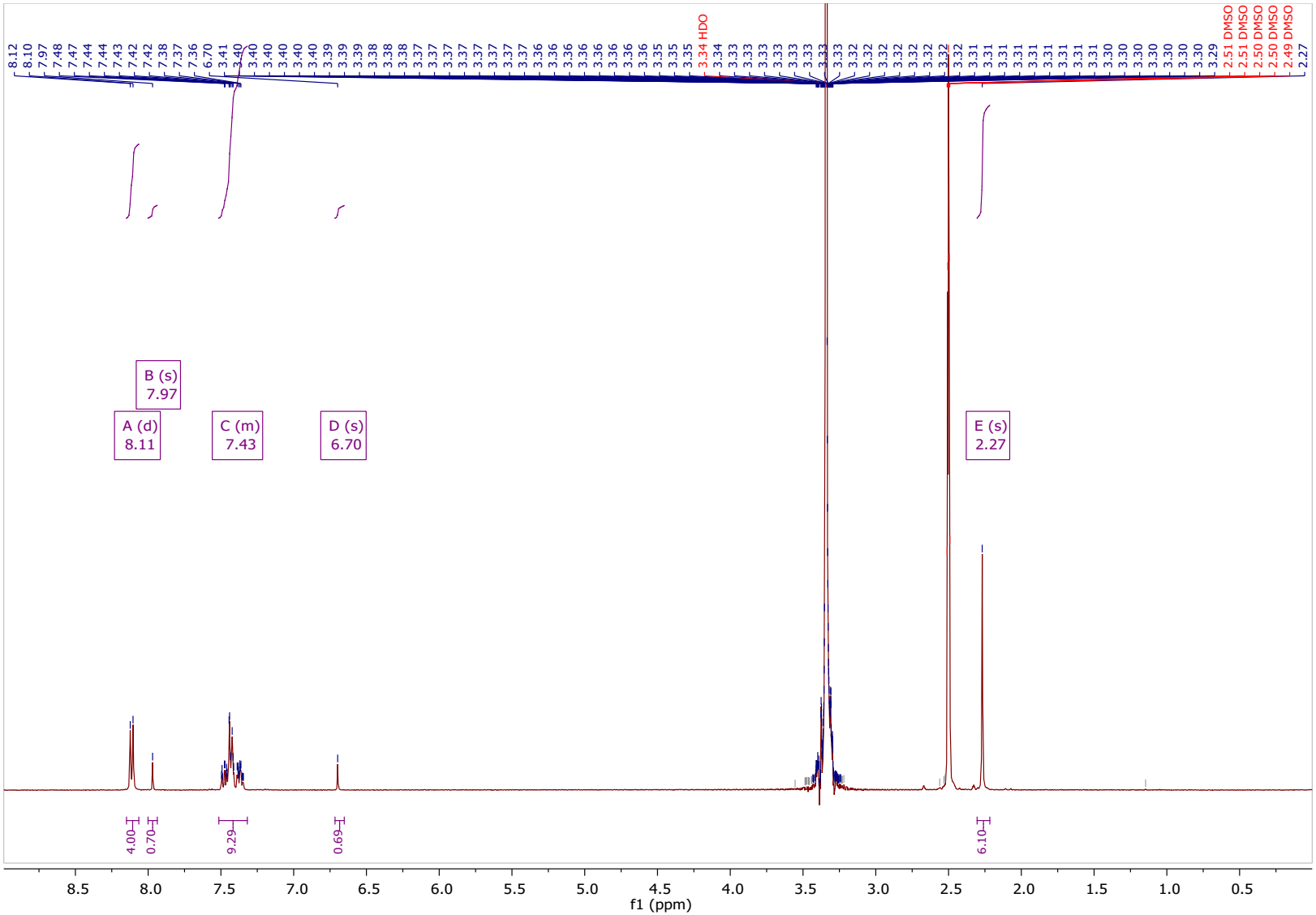

Figure S19 ^{1}H NMR spectrum of complex [Bi(*p*-tol)$_2$(O(O)P(H)Ph)]$_n$ **10** in d$_6$-DMSO.

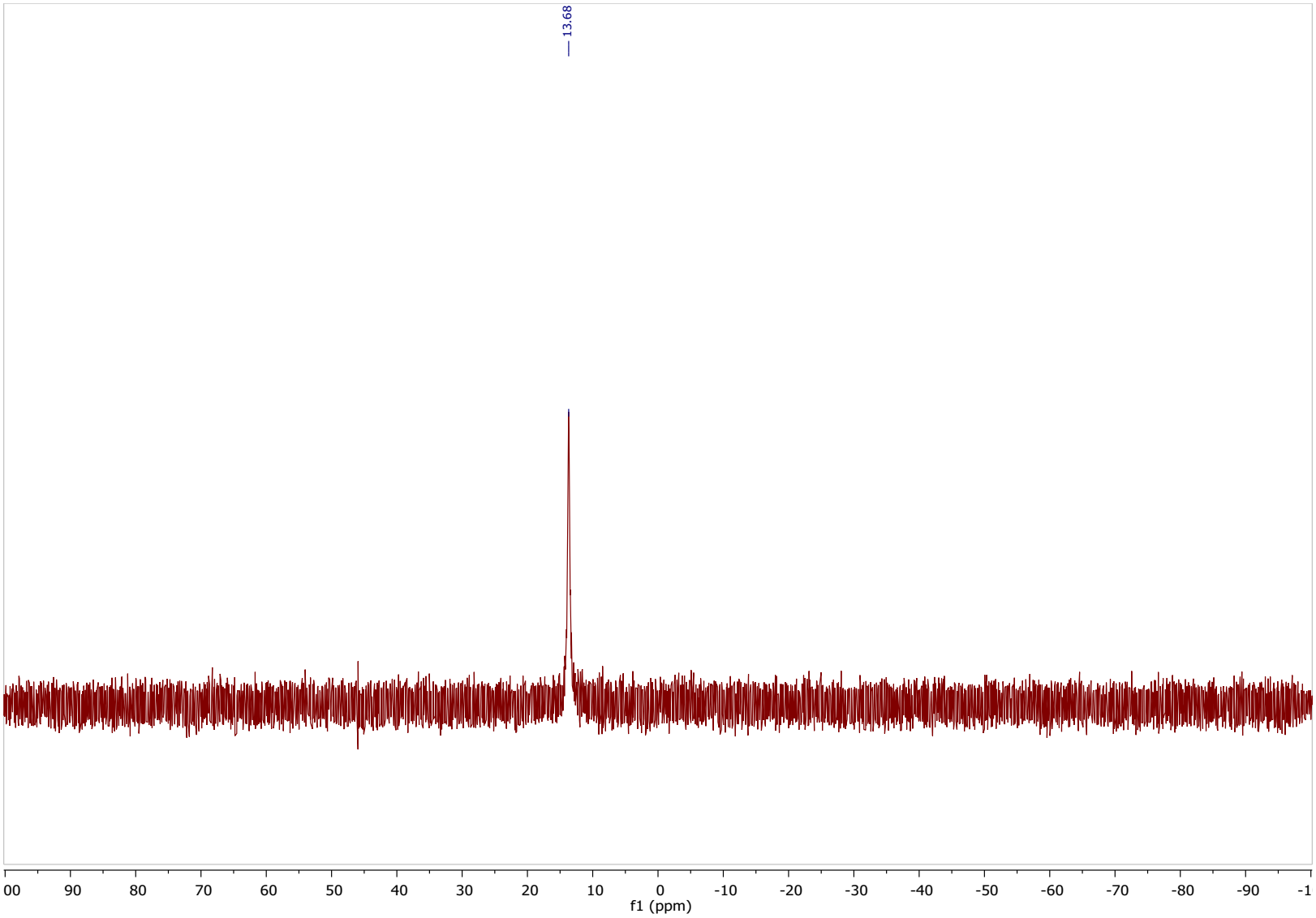

Figure S20 ^{31}P NMR spectrum of complex [Bi(*p*-tol)$_2$(O(O)P(H)Ph)]$_n$ **10** in d$_6$-DMSO.

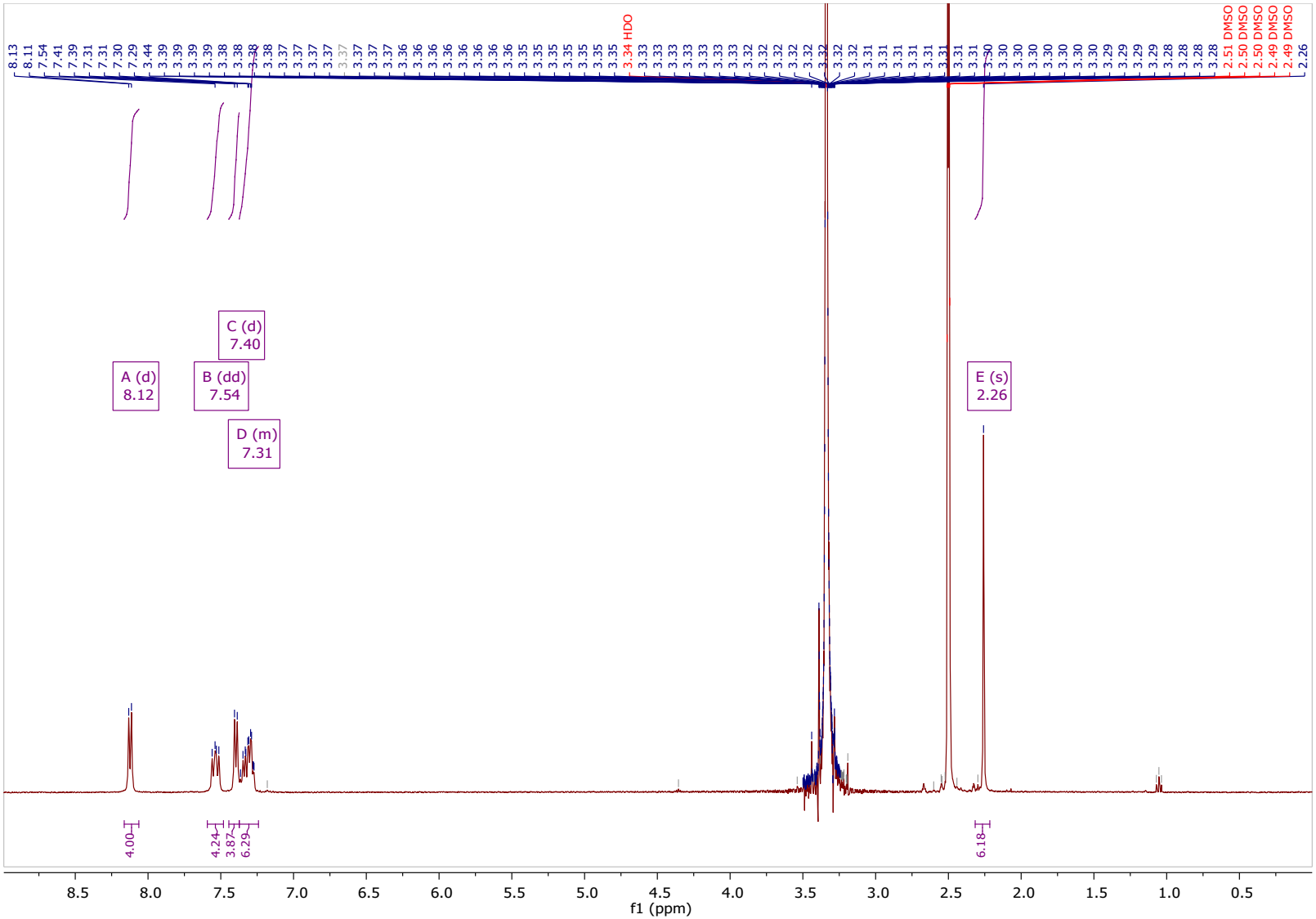

Figure S21 ^{1}H NMR spectrum of complex $[Bi(p\text{-tol})_2(O(O)PPh_2)]_n$ **11** in d_6-DMSO.

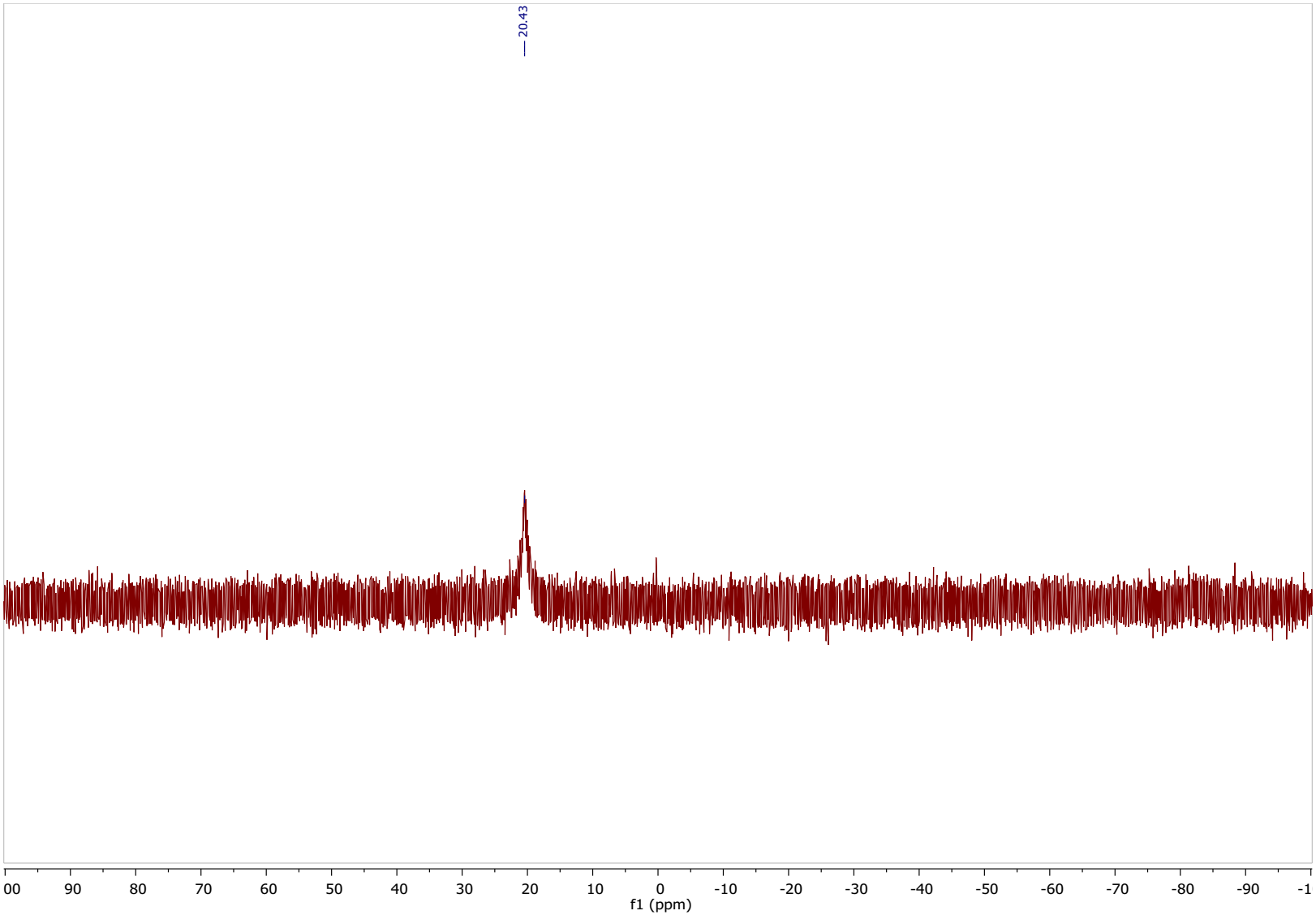

Figure S22 ^{31}P NMR spectrum of complex [Bi(*p*-tol)$_2$(O(O)PPh$_2$)]$_n$ **11** in d$_6$-DMSO.

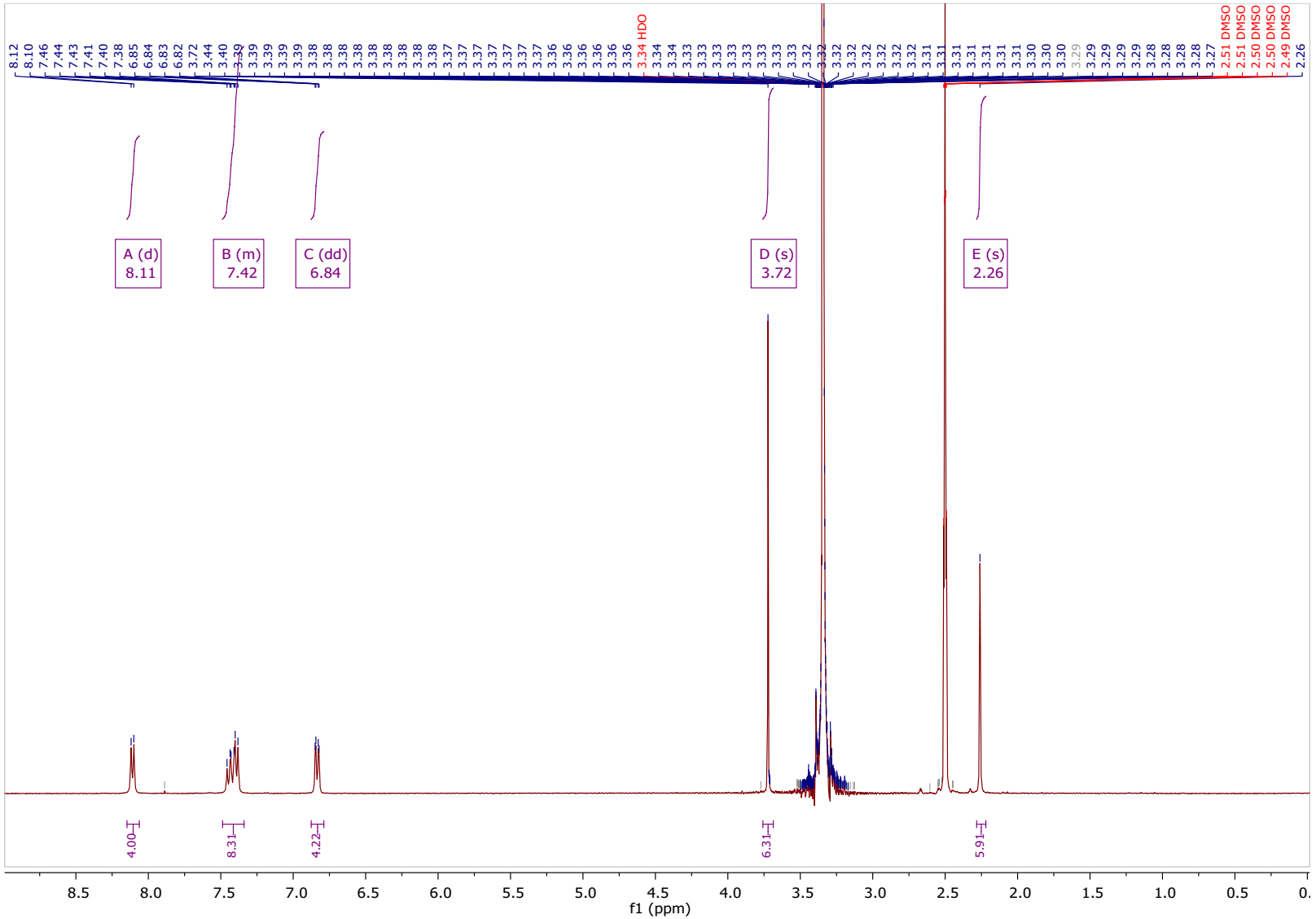

Figure S23 ^{1}H NMR spectrum of complex [Bi(*p*-tol)$_2$(O(O)P(*p*-MeOPh)$_2$)]$_n$ **12** in d$_6$-DMSO.

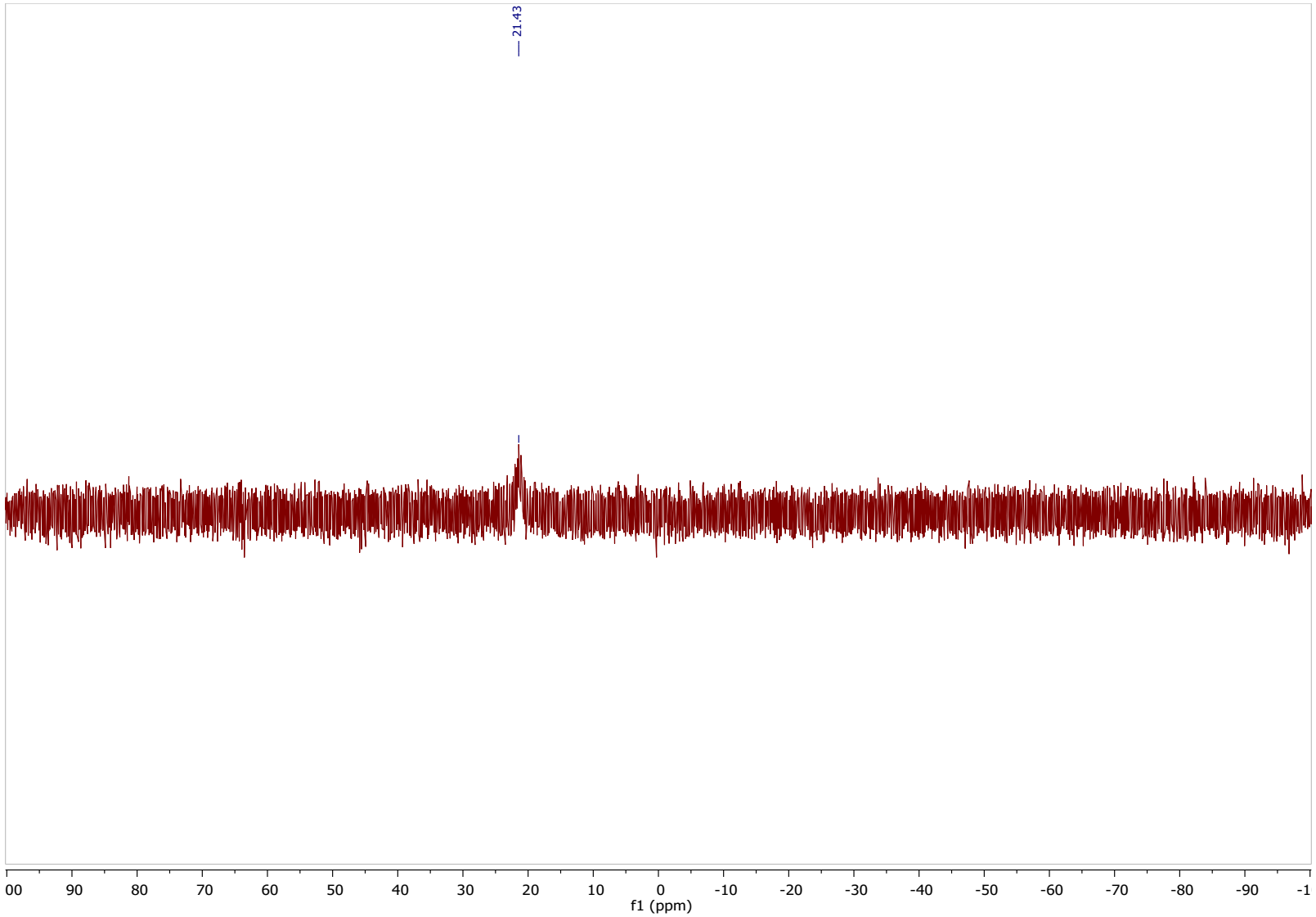

Figure S24 ^{31}P NMR spectrum of complex $[Bi(p\text{-tol})_2(O(O)P(p\text{-MeOPh})_2)]_n$ **12** in d_6-DMSO.

Table S1 Characterisation of complexes **1** – **12** compared with their parent phosphinic acids including difference in asymmetric and symmetric PO_2 stretching as determined by IR, and melting temperatures as determined by DSC-TGA.

Compound		**Δ*ν* (cm^{-1})**	**Melting point (°C)**
$[Bi(o\text{-}MeOPh)_2(O(O)P(H)Ph)]_n$	**1**	94, 105	149*
$[Bi(o\text{-}MeOPh)_2(O(O)PPh_2)]_n$	**2**	110, 111	177*
$[Bi(o\text{-}MeOPh)_2(O(O)P(p\text{-}MeOPh)_2)]_n$	**3**	107, 112	186*
$[Bi(m\text{-}MeOPh)_2(O(O)P(H)Ph)]_n$	**4**	91, 98	127
$[Bi(m\text{-}MeOPh)_2(O(O)PPh_2)]_n$	**5**	111, 130	161*
$[Bi(m\text{-}MeOPh)_2(O(O)P(p\text{-}MeOPh)_2)]_n$	**6**	92, 110	151
$[Bi(m\text{-}tol)_2(O(O)P(H)Ph)]_n$	**7**	90, 100	139
$[Bi(m\text{-}tol)_2(O(O)PPh_2)]_n$	**8**	75, 98	152
$[Bi(m\text{-}tol)_2(O(O)P(p\text{-}MeOPh)_2)]_n$	**9**	98, 99	239*
$[Bi(p\text{-}tol)_2(O(O)P(H)Ph)]_n$	**10**	108, 130	156*
$[Bi(p\text{-}tol)_2(O(O)PPh_2)]_n$	**11**	88, 93	219*
$[Bi(p\text{-}tol)_2(O(O)P(p\text{-}MeOPh)_2)]_n$	**12**	101, 108	188*
$Ph(H)P(O)OH$		164	
$Ph_2P(O)OH$		168	
$(p\text{-}MeOPh)_2P(O)OH$		177	

‡ Denotes solid-state ^{31}P NMR. * Denotes decomposition point.

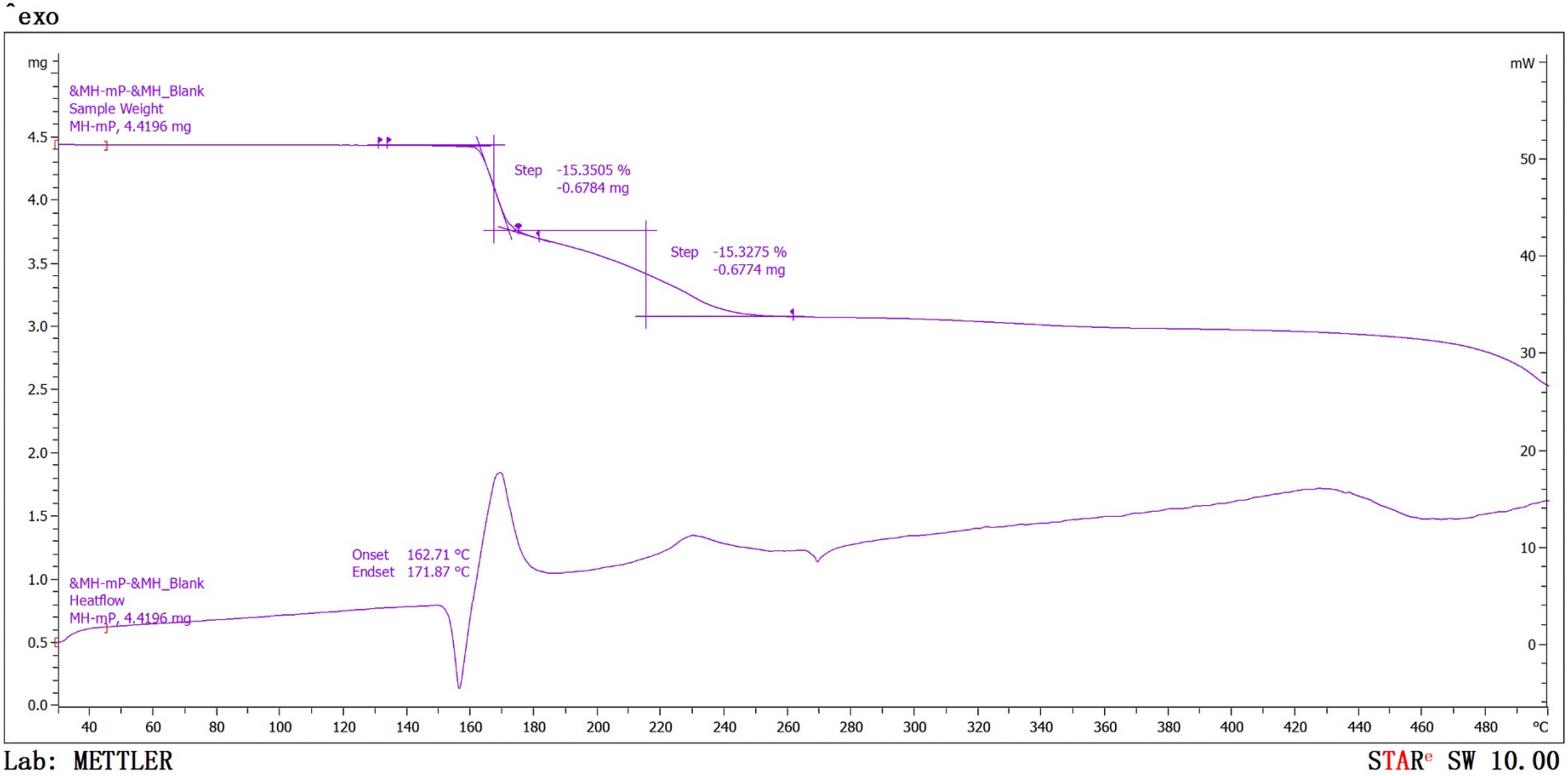

Figure S25 TGA trace of complex [Bi(*m*-MeOPh)$_2$(O(O)P(H)Ph)]$_n$ **4**, showing the loss of two methoxyphenyl moieties. DSC trace is shown below.

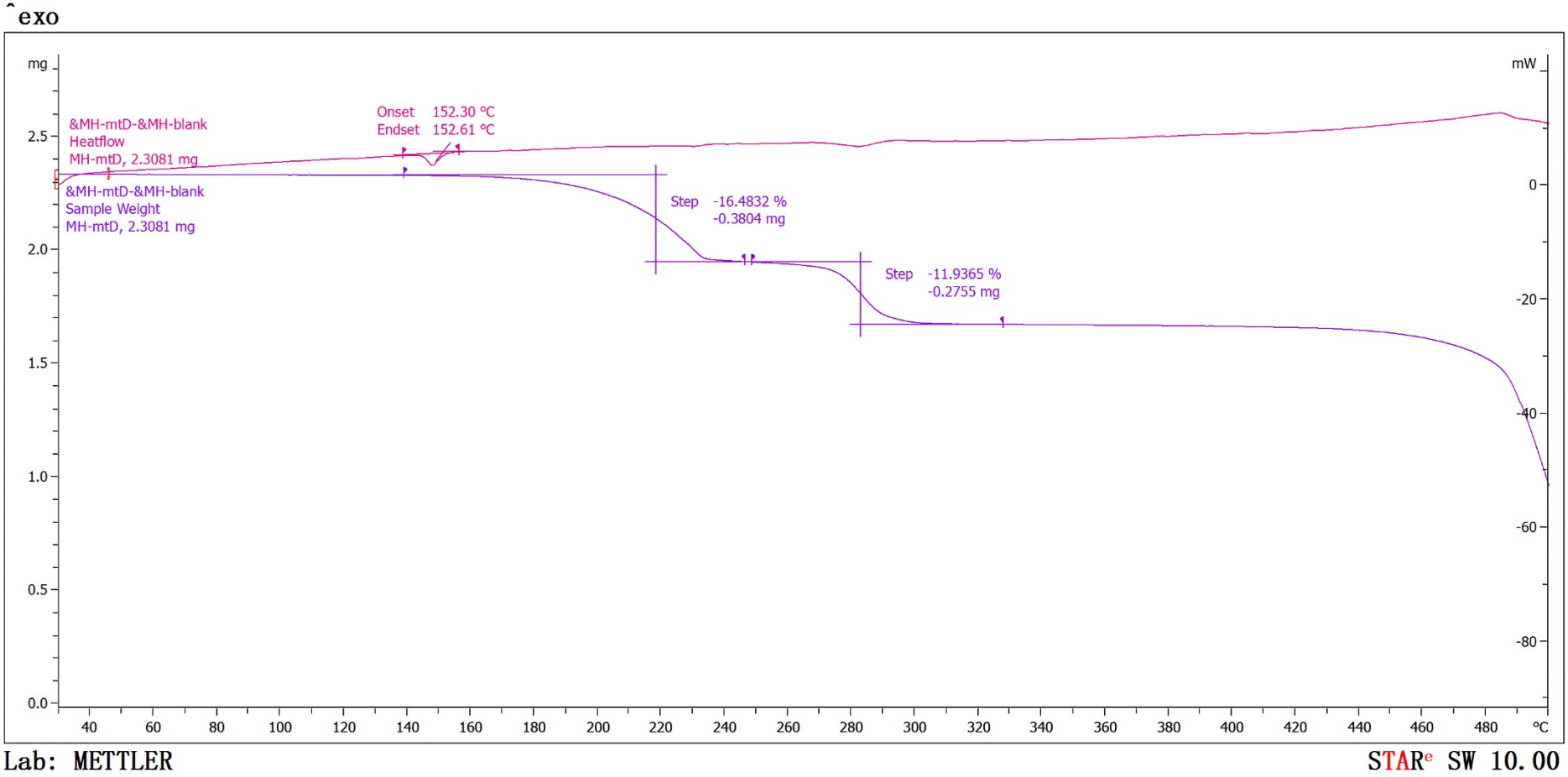

Figure S26 TGA trace (purple) of complex $[Bi(m\text{-tol})_2(O(O)PPh_2)]_n$ **8**, showing the loss of two tolyl moieties. DSC trace is shown in pink.

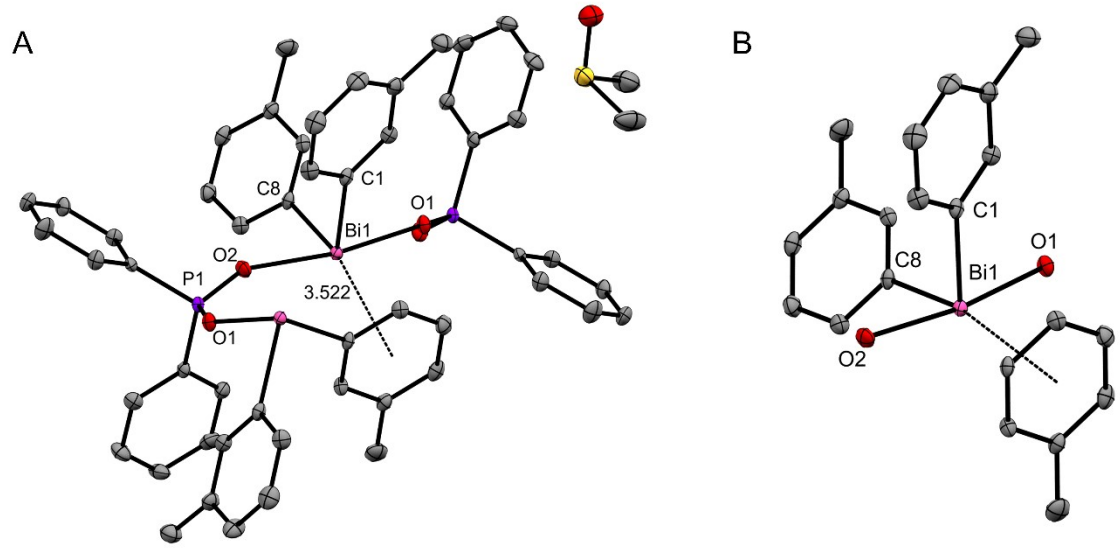

Figure S27 Polymeric structure of ([Bi(*m*-tol)$_2$(O(O)PPh$_2$)].DMSO)$_n$ **8** (A) with DMSO in the lattice, and geometry around the bismuth centre (B) showing the distorted square pyramidal confirmation with evidence of a sterically active lone pair. Thermal ellipsoids shown at 50 % probability with hydrogen atoms omitted for clarity. Selected bond lengths (Å) and angles (°): Bi1-O1 2.3238(17); Bi1-O2 2.3742(17); Bi1-C1 2.255(2); Bi1-C8 2.264(2); Bi1-arene$_{centroid}$ 3.522; O1-Bi1-O2 172.23(6); O1-Bi1-C1 86.30(8); O1-Bi1-C8 90.07(8); O2-Bi1-C1 88.51(8); O2-Bi1-C8 84.42(7); C1-Bi1-C8 92.93(9); C8-Bi1-arene$_{centroid}$ 169.04. Symmetry operator: (-x + 1/2, y + 1/2, -z + 1/2).

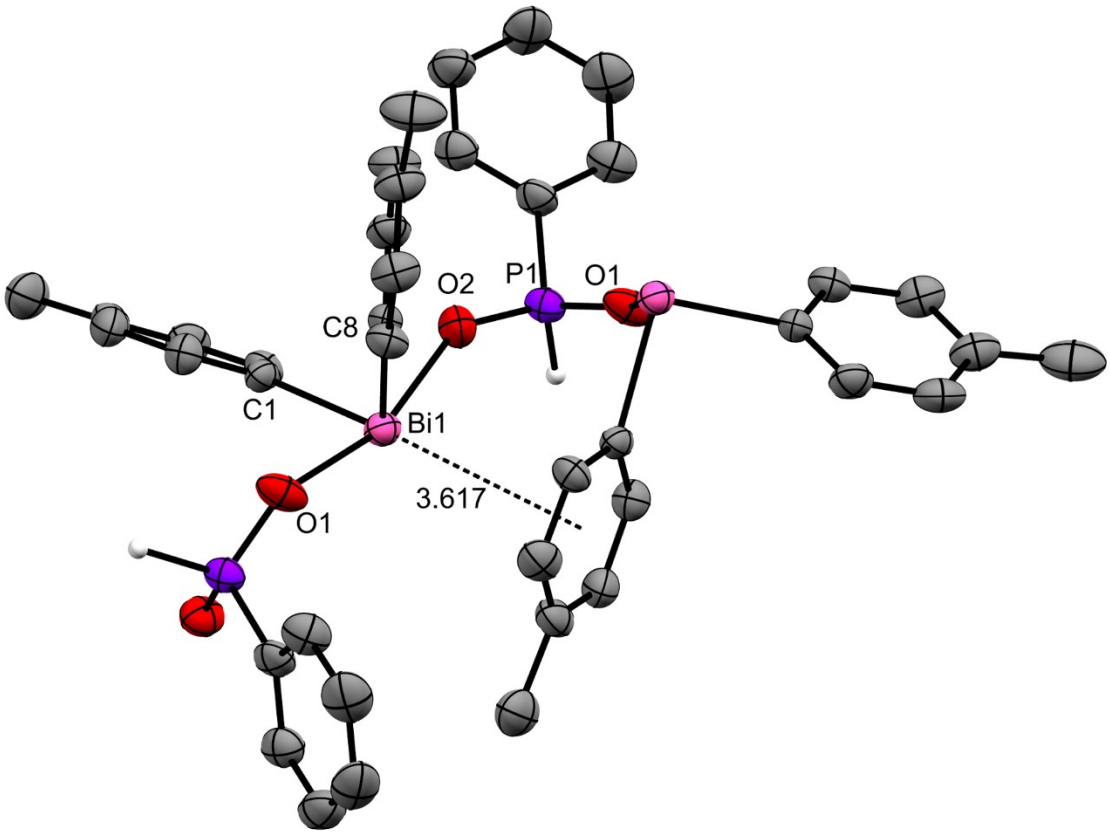

Figure S28 Molecular structure of complex [Bi(*p*-tol)$_2$(O(O)P(H)Ph)]$_n$ **10**. Thermal ellipsoids shown at 50 % probability with aromatic hydrogen atoms omitted for clarity. Selected bond lengths (Å) and angles (°): Bi1-O1 2.350(5); Bi1-O2 2.361(5); Bi1-C1 2.245(6); Bi1-C8 2.226(6); Bi1-arene$_{centroid}$ 3.617; O1-Bi1-O2 162.66(18); O1-Bi1-C1 86.2(2); O1-Bi1-C8 82.19(18); O2-Bi1-C1 82.60(19); O2-Bi1-C8 85.49(18); C1-Bi1-C8 94.5(2); C1-Bi1-arene$_{centroid}$ 171.25. Symmetry operator: (-x + 1/2, y - 1/2, -z + 3/2).

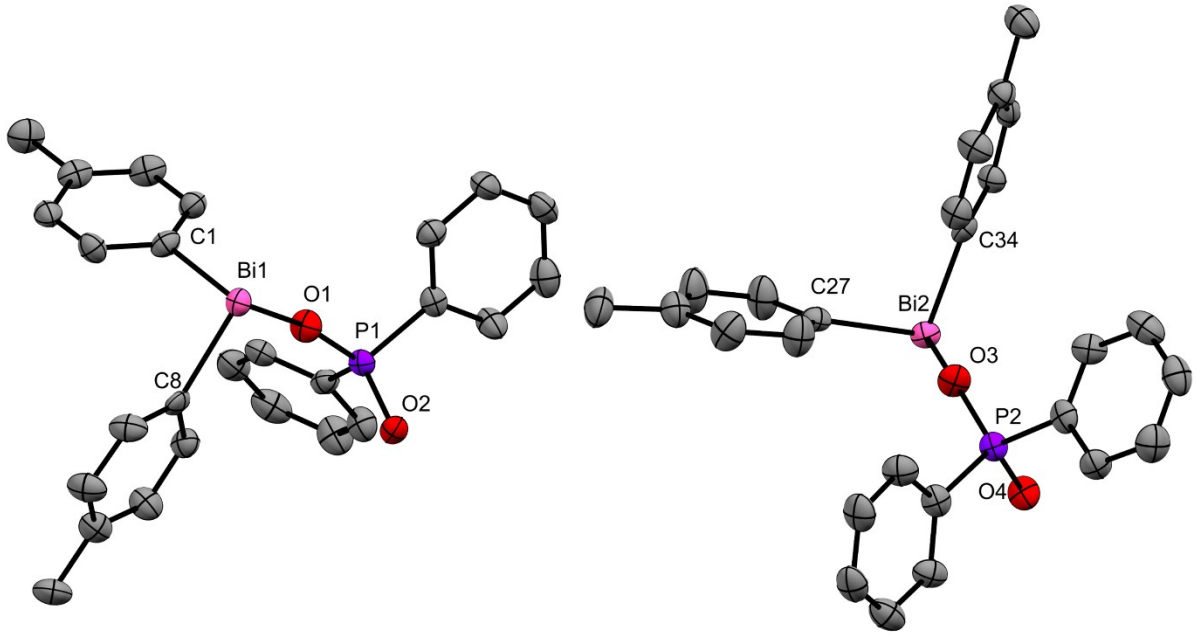

Figure S29 Molecular structures of complex $[Bi(p\text{-tol})_2(O(O)PPh_2)]_n$ **11**. Thermal ellipsoids shown at 50 % probability with hydrogen atoms omitted for clarity. Selected bond lengths (Å) and angles (°): Bi1-O1 2.379(6); Bi1-O2 2.329(6); Bi1-C1 2.272(8); Bi1-C8 2.254(9); Bi1-arene$_{centroid}$ 3.429; Bi2-O3 2.355(6); Bi2-O4 2.361(6); Bi2-C27 2.262(9); Bi2-C34 2.249(10); Bi1-arene$_{centroid}$ 3.509; O1-Bi1-O2 172.1(2); O1-Bi1-C1 84.4(3); O1-Bi1-C8 90.2(3); O2-Bi1-C1 89.0(3); O2-Bi1-C8 85.5(3); C1-Bi1-C8 90.8(3); C1-Bi1-arene$_{centroid}$ 171.16; O3-Bi2-O4 171.2(2); O3-Bi2-C27 85.8(3); O3-Bi2-C34 86.4(3); O4-Bi2-C27 87.8(3); O4-Bi2-C34 88.0(3); C27-Bi2-C34 93.2(3); C27-Bi2-arene$_{centroid}$ 90.20. Symmetry operator: Bi1 (-x + 1, y + 1/2, -z + 2) and Bi2 (-x, y + 1/2, -z + 1).

Table S2 Minimum inhibitory concentrations (MICs) of triaryl bismuth reagents ($BiAr_3$) to inhibit ≥ 80 % growth of MRSA, VRE, *E. coli*, and *P. aeruginosa*, as measured by absorbance at 600 nm following overnight incubation at 37 °C.

Compound	**MIC (μM)**			
	MRSA	VRE	*E. coli*	*P. aeruginosa*
Bi(*o*-MeOPh)$_3$	> 100	> 100	> 100	> 100
Bi(*m*-MeOPh)$_3$	> 100	> 100	> 100	> 100
Bi(*m*-tol)$_3$	> 100	> 100	> 100	> 100
Bi(*p*-tol)$_3$	> 50	> 50	> 50	> 50

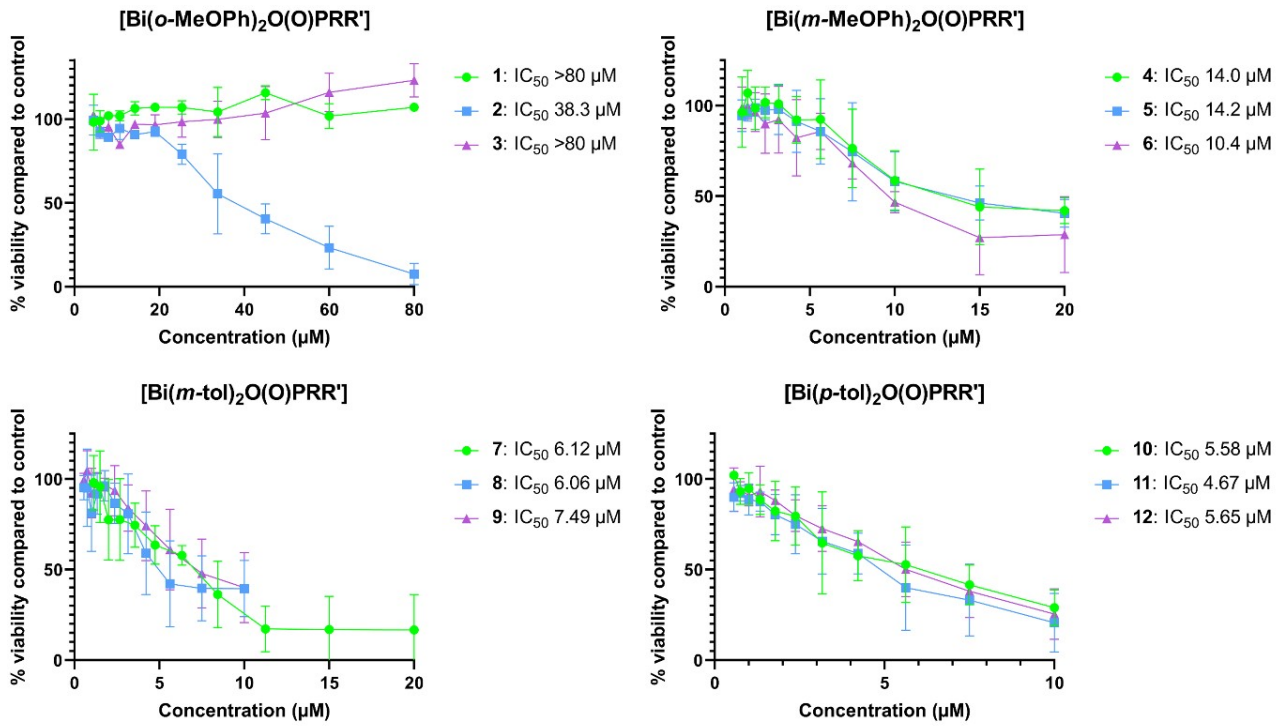

Figure S30 Cos-7 viability following 24 hour incubation at 37 °C, 5 % CO_2 with complexes **1** – **12**.

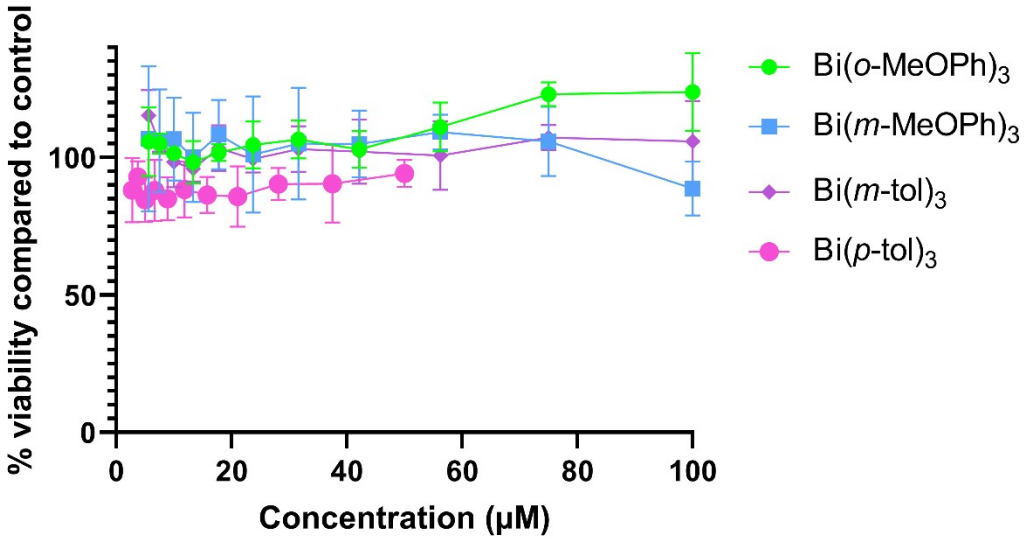

Figure S31 Cos-7 viability following 24 hour incubation at 37 °C, 5 % CO_2 with $BiAr_3$.

Table S3 Summary of crystallographic data for complexes **4**, **7**, **8**, **10** and **11**.

Complex	[Bi(*m*-MeOPh)$_2$O(O)P(H)Ph] **4**	[Bi(*m*-tol)$_2$O(O)P(H)Ph] **7**	[Bi(*m*-tol)$_2$O(O)PPh$_2$] .DMSO **8**	[Bi(*p*-tol)$_2$O(O)P(H)Ph] **10**	[Bi(*p*-tol)$_2$O(O)PPh$_2$] **11**
CCDC	2130070	2130069	2130071	2130072	2130073
Formula	$C_{20}H_{20}BiO_4P$	$C_{20}H_{20}BiO_2P$	$C_{26}H_{24}BiO_2P$, C_2H_6OS	$C_{20}H_{20}BiO_2P$	$C_{26}H_{24}BiO_2P$
Formula weight	564.31	532.31	686.53	532.31	608.40
Crystal system	Orthorhombic	Monoclinic	Monoclinic	Monoclinic	Monoclinic
Space group	$P2_12_12_1$	$P2_1$	$P2_1/n$	C2/c	$P2_1$
a (Å)	9.4175(4)	8.7590(18)	14.2607(2)	18.7237(4)	11.7325(2)
b (Å)	9.4368(3)	9.4710(19)	10.1056(2)	9.2659(2)	9.3795(2)
c (Å)	21.9641(6)	11.418(2)	18.4960(4)	23.2109(5)	10.9611(5)
α (°)	90	90	90	90	90
β (°)	90	99.95(3)	95.6810(10)	107.783(5)	96.470(2)
γ (°)	90	90	90	90	90
Volume (Å^3)	1951.97(12)	932.9(3)	2652.42(9)	3834.50(15)	2291.97(8)
Z	4	2	4	8	4
Density (g cm^{-3})	1.920	1.895	1.719	1.844	1.763
μ (mm^{-1})	9.136	9.543	6.813	18.902	7.782
F_{000}	1080	508	1344	2032	1176
T (K)	123(2)	293(2)	123.00(10)	122.99(10)	123.00(10)
$2\theta_{max}$ (◦)	56.6	57.1	62.1	160.0	52.7
Reflections collected	18660	11397	34988	20042	25295
Unique reflections	4810 (R_{int} = 0.0462)	3692 (R_{int} = 0.0198)	7568 (R_{int} = 0.0455)	4101 (R_{int} = 0.0622)	9013 (R_{int} = 0.0373)
Final GooF	1.044	1.173	1.083	1.031	1.013
R_1	0.0264	0.0184	0.0240	0.0386	0.0310
wR_2 (all data)	0.0482	0.0475	0.0574	0.1282	0.0789
Flack parameter	-0.038(6)	-0.017(3)	-	-	-0.021(5)